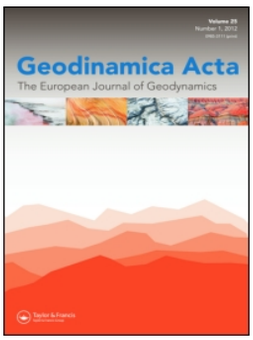

Geodinamica Acta

ISSN: 0985-3111 (Print) 1778-3593 (Online) Journal homepage: https://www.tandfonline.com/loi/tgda20

Geochemistry and Tectonic Implications of Leucogranites and Tourmalines of the Southern Menderes Massif, Southwest Turkey

Erdin Bozkurt , John A. Winchester , Steven K. Mittwede & Christopher J. Ottley

To cite this article: Erdin Bozkurt , John A. Winchester , Steven K. Mittwede & Christopher J. Ottley (2006) Geochemistry and Tectonic Implications of Leucogranites and Tourmalines of the Southern Menderes Massif, Southwest Turkey, Geodinamica Acta, 19:5, 363-390, DOI: 10.3166/ga.19.363-390

To link to this article: https://doi.org/10.3166/ga.19.363-390

Published online: 13 Apr 2012.

Geodinamica Acta

Geodinamica Acta 19/5 (2006) 363-390

Geochemistry and Tectonic Implications of Leucogranites and Tourmalines of the Southern Menderes Massif, Southwest Turkey

Erdin Bozkurt [a]*, John A. Winchester [b], Steven K. Mittwede [c] & Christopher J. Ottley [d]

[a] *Middle East Technical University, Department of Geological Engineering, Tectonic Research Unit, TR–06531 Ankara, Turkey*
[b] *Keele University, School of Physical and Geographical Sciences, Earth Sciences and Geography, Staffordshire ST5 5BG, England*
[c] *Müteferrika Consulting Services Ltd., P.K. 290, Yenişehir, TR–06443 Ankara, Turkey*
[d] *Department of Geological Sciences, Science Laboratories, South Road,Durham DH1 3LE, England*

Received: 15/02/05, accepted: 17/05/06

Abstract

Granitoid rocks of the southern Menderes Massif, SW Turkey include widespread possibly Ediacaran high-grade granitic orthogneisses and younger (Tertiary) sheets, sills and/or dikes of variably deformed tourmaline-bearing leucogranites. The latter are confined to the immediate footwall of the regional-scale ductile southern Menderes shear zone. Although both sets of granitoid rocks are essentially calc-alkaline and peraluminous, the syn- to post-collisional tourmaline-bearing leucogranites are chemically distinguishable from both the granitoid orthogneisses and from two sets of mostly sodic siliceous dyke rocks. The leucogranites were generated by partial melting induced by shear heating during the waning stages of the Eocene main Menderes metamorphism and associated top-to-the-NNE thrusting along the southern Menderes ductile shear zone, which transported schists northwards over the granitoid orthogneisses of the core Menderes complex. Upward migration and emplacement of leucogranitic melt weakened formerly sheared rocks, so that when thrust-related deformation ceased it facilitated rapid crustal extension along the shear zone. The emplacement of leucogranites, in turn, promoted the reactivation of the southern Menderes shear zone as a top-to-the-SSW extensional feature. Continued extensional deformation affected the leucogranites which became parallel to the shear-zone foliation; local S-C fabrics were also generated. The additional occurrence of less or almost undeformed leucogranites suggests that the latest stages of extension might have induced adiabatic decompressional melting. Hence the leucogranite melt generation and emplacement in the southern Menderes Massif occurred in pulses. Both compressional and extensional processes played key roles in melt generation, emplacement, deformation and exhumation of the massif.

A clear distinction may also be made between the composition of granite-hosted tourmalines and those from metasedimentary schists. Tourmalines from a pebble of uncertain provenance in the Gökçay metaconglomerate plotted with schist-hosted tourmalines, suggesting that it was unlikely to be derived from granitoid gneiss. This crucial piece of evidence suggests that the presence of a major (Pan-African) unconformity at the so-called "core (orthogneiss)-cover (schist)" boundary in the southern Menderes Massif is unnecessary.

Keywords: leucogranites, torumaline, extension, exhumation, shear zone, geochemistry, Menderes Massif, Turkey

1. Introduction

Granites have been used extensively to establish the interplay between crustal thickening and extensional exhumation of metamorphic terranes in collisional orogens [e.g., 1–15]. Such records involve significant crustal thickening, widespread migmatization and granitic magma generation, and large-scale extension along detachments faults/extensional shear zones.

* Corresponding author.
E-mail address: erdin@metu.edu.tr

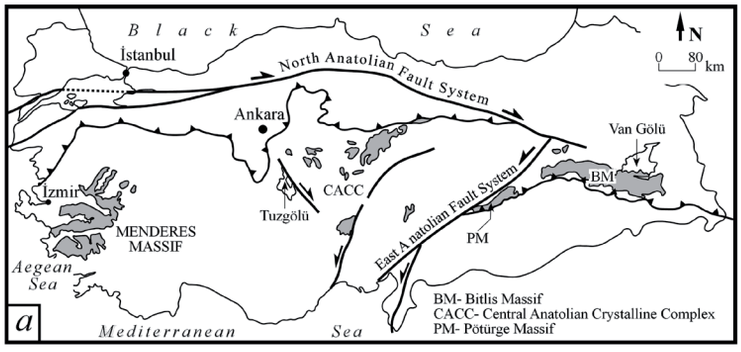

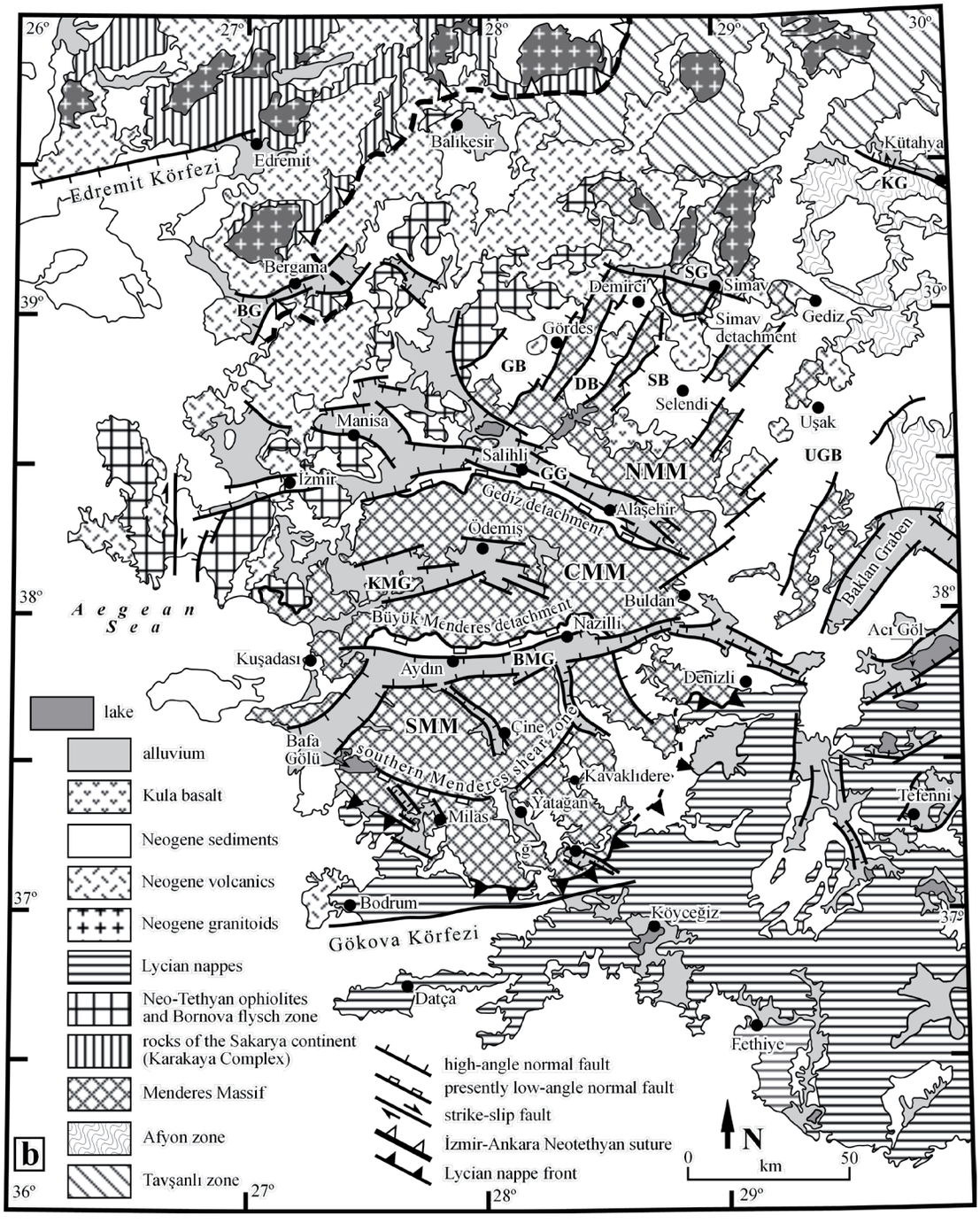

Figure 1:
(a) Simplified geological map of Turkey showing the major metamorphic massifs and fault zones. BM– Bitlis Massif, CACC– Central Anatolian Crystalline Complex, PM– Pulur Massif (from Whitney & Bozkurt [74]).
(b) Geological map of western Turkey showing the Menderes Massif and its subdivision. The distribution of rock units are simplified from MTA 1:500 000-scale geological maps, İzmir and Denizli sheets, Okay & Tüysüz [150], Okay [151], Beccaletto & Jenny [152], Duru *et al.* [153], Okay & Altıner [154], Okay & Göncüoğlu [155], Pickett & Robertson [156].
BG– Bakırçay Graben; DB– Demirci Basin; GB– Gördes Basin; GG– Gediz Graben; KG– Kütahya Graben; SB– Selendi Basin; SG– Simav Graben; BMG– Büyük Menderes Graben; CMM– Central Menderes Massif; KMG– Küçük Menderes Graben; BMM– Northern Menderes Massif; SMM– Southern Menderes Massif; UGB– Uşak-Güre Basin.

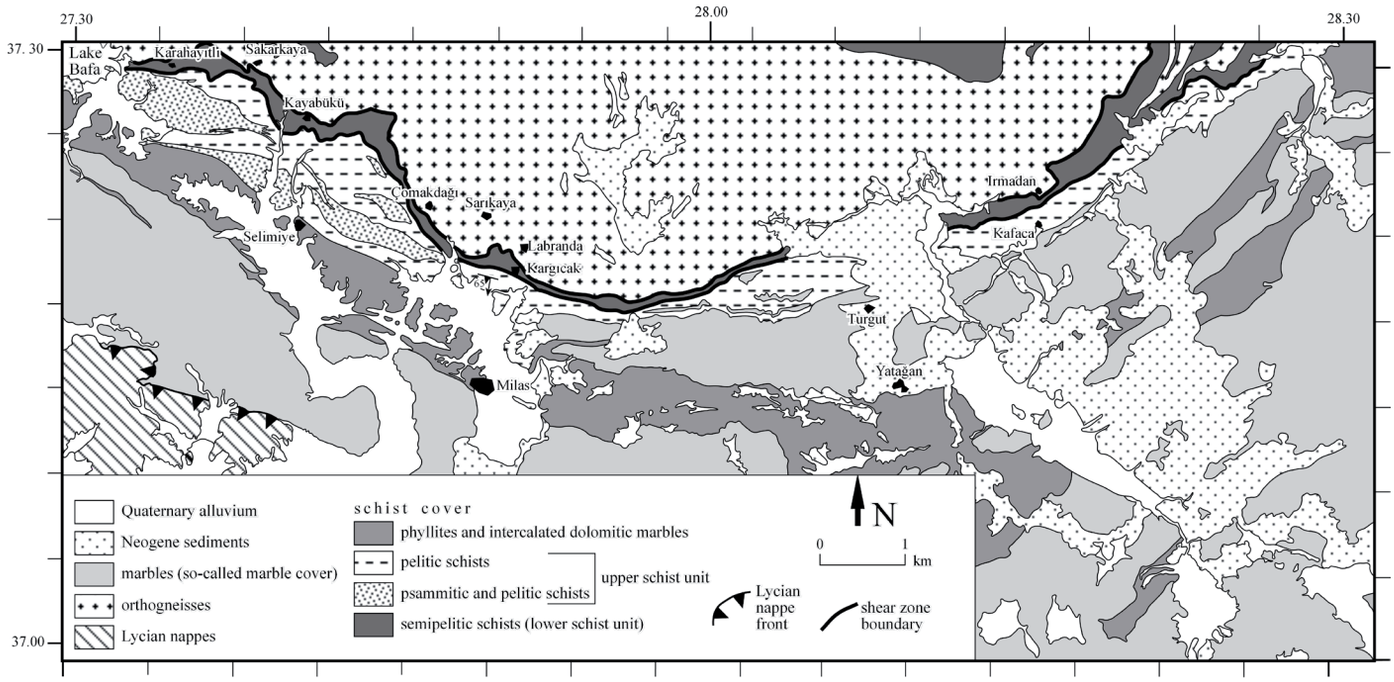

Figure 2: Geological map of the southern Menderes Massif (simplified from MTA 1:100 000-scale geological maps, sheets N19, N20; Neşat Konak).

Widespread granite emplacement in the immediate footwall of these structures has therefore been attributed to, and is commonly used to date the timing of, large-scale syn- to post-orogenic extension or orogenic collapse (e.g., Himalayas [6, 16–19], Variscan Belt of central northern Portugal [20], Variscan Belt of Spain [21], Proterozoic of Greenland [22], North American Cordillera [23, 24], Canadian Cordillera [25–28], Caledonides [13 and references therein], French Massif Central [29 and references therein], Aegean [30–33 and references therein]).

The Menderes Massif in southwestern Turkey is a product of a major end-Oligocene–Miocene crustal extension, following Palaeogene crustal thickening related to continental shortening during the closure of the Neotethyan ocean between the Sakarya continent in the north and the Anatolian-Tauride platform in the south [e.g., 34–52]. The massif comprises three distinct submassifs, separated by the modern Büyük Menderes and Gediz grabens: the southern (Çine), central (Ödemiş-Kiraz) and northern (Gördes) submassifs, each of which was exhumed in the footwall of what are now low- to moderate-angle normal ductile-to-brittle shear/fault zones (Fig. 1). The footwall rocks consist mainly of high-grade metasedimentary rocks and/or metamorphosed granitoids, separated from a hanging wall (low-grade metasediments and/or unmetamorphosed Miocene continental clastic sediments) by brittle, now low-angle normal fault(s)/detachments. The massif is therefore interpreted as a crustal-scale metamorphic core complex and forms the heart of the highly extended southwestern Turkey extensional province. A horst-and-graben structure, with regional ~E–W-trending grabens (e.g., Büyük Menderes and Gediz grabens) and intervening horsts, form the other conspicuous elements of the region [e.g., 53–67]. Because southwestern Turkey is one of the best localities in the world to study extensional tectonics, the Menderes Massif and modern grabens have been the subject of many studies during the last two decades. Most research has addressed the issues of core-complex formation and evolution, volcanism, normal faulting, graben formation and associated deformation. The occurrence of syn-extensional granitoids has been well documented from the northern and central submassifs (e.g., Eğrigöz and Koyunoba granitoids: Işık & Tekeli [47], Işık *et al*. [49], Ring & Collins [52]; Salihli granitoid: Hetzel *et al*. [38]). In those studies, these granites were used to date the initiation of crustal extension in southwestern Turkey, but there has been almost no research to address the crucial role of and interplay between metamorphism, granitic magma generation (crustal melting) and emplacement, and normal faulting (orogenic collapse) in the exhumation history of the metamorphic rocks of the Menderes Massif.

In this communication, we report on the field relations, petrography and geochemical characteristics of granitoid rocks of the southern Menderes Massif to fill the gap described above. The southern submassif comprises two distinct rock bodies juxtaposed along a structural discontinuity: (i) metamorphosed granitoid rocks (orthogneisses) in the footwall to the north and (ii) a high- to low-grade Palaeozoic–Cenozoic metasedimentary sequence in the hanging wall to the south [e.g., 41, 44, 68 and references therein]. The former are traditionally known as '*core*' rocks while the latter is interpreted as *cover*. The tectonic contact, the southern Menderes shear zone (SMSZ), is interpreted as a kilometre-scale, down-to-the-S–SSW, ductile-to-brittle Alpine shear zone, and is a prominent feature from Lake Bafa in the west to Yatağan in the east [42] (Fig. 2). The massif displays evidence for polyphase metamorphism: Early high pressure (M_1) metamorphic assemblages occur as a

Fe-Mg-carpholite-chloritoid paragenesis and record *P-T* conditions of about 440 ºC and 10–12 kbar [69, 70], whereas a later HT/MP Barrovian-type regional metamorphic (M_2) assemblage records conditions of 430–> 550 ºC and 5–7 kbar [71–76]. The last phase of metamorphism (M_3) occurred in the footwall of the southern Menderes shear zone under decreasing *P-T* conditions (greenschist-facies and anchizone conditions).

The granitoid rocks in the footwall of the southern Menderes shear zone comprise two contrasting peraluminous granitic bodies: (i) older (possibly Precambrian) widespread high-grade granitic orthogneisses, traditionally known as augen gneisses; (ii) younger (undated, presumably Tertiary) leucocratic metagranite [41] confined to the regional-scale ductile southern Menderes shear zone, occurring generally as sheets, sills and/or dikes. The southern Menderes Massif in southwestern Turkey is therefore a crustal-scale metamorphic culmination characterized by the production of granitic melts and leucogranite emplacement in the immediate footwall of a crustal-scale extensional shear zone, and is a place where models of granitic-magma generation and emplacement in an extensional tectonic setting can be tested and investigated. We think that study of the granitic rocks of the southern Menderes Massif will lead to a better understanding of: (i) the structural and thermal evolution of thickened crust in collisional settings, (ii) granitic-magma generation and emplacement, and (iii) subsequent orogenic collapse

This paper first describes briefly the geology and petrography of granitic rocks of the southern Menderes exposed around Yatağan area. Geochemical data then documents the distinctive chemical characteristics of the orthogneisses and leucogranites in order to elucidate their tectonic settings. The paper also details geochemical characteristics of tourmalines both in the granitoids and in the pebbles of reported metaconglomerates of metasediments to comment on their significance about the contact relations between granitoids and structurally overlying metasediments. Finally, available structural, metamorphic and geochronological data are combined to discuss the mechanism of granitic-melt generation and possible emplacement mechanisms of younger leucogranites within the context of the tectonomagmatic evolution of the southern Menderes Massif. The nature of the granitoid-schist contact will also be discussed.

2. Current Problems

Although research into the tectonometamorphic evolution and exhumation of the southern Menderes Massif has increased dramatically since the work by Bozkurt & Park [34], there is still no established consensus concerning its evolution. Controversies centre on the age of granitic rocks (orthogneisses) and the nature of their contact relationships with structurally overlying metasediments. Similarly, the age of the top-to-the-NNE fabrics in the orthogneisses is also debated.

Several studies claimed that granitoids have intruded the high-grade metasediments during Tertiary time [34–36, 77–86]. According to those workers, there is evidence for weak contact metamorphism in the Mesozoic carbonates [80, 81, 86] and in the Palaeozoic schists [78–80, 83, 84, 87, 88]. Contrary to this view, others argued, based on geochronological data (c. 521 and 572 Ma, averaging 550 Ma, by U–Pb and Pb–Pb single zircon evaporation methods), that the granitic protoliths were emplaced during Late Precambrian–Early Cambrian time [e.g., 45, 89–92]. These authors refuted cross-cutting relationships, except for the area along the eastern shore of Lake Bafa, which they thought indicated the presence of Precambrian metasediments in the so-called '*cover*' sequence [89]. The orthogneisses yield a wide scatter of zircon U–Pb ages in the range of 2555–521 Ma; accordingly they are interpreted as representing a fragment of Pan-African basement in the Menderes Massif [45, 89, 91–96]. Also, one zircon grain from the foliated quartzite of the '*cover'* rocks yielded an age of 526±2 Ma [91]; this rock is cut by granitic rocks around Sakarkaya village. These zircon ages therefore conflict with the field relations, thus casting serious doubt on the reliability and significance of the recent single-grain zircon ages.

More recently, there have been three more attempts to present a suitable explanation of the age and boundary relations of granitic rocks of the submassif. Gessner *et al*. [97] have dated two granitic rock samples from along the eastern shore of the Lake Bafa and from the Eskiçine area. The U–Pb SIMS dating of this granite on a SHRIMP II yielded weighted mean ages of 541±14 Ma and 566±9 Ma, respectively, which they interpreted as granite crystallization ages. Those authors reported that the granite samples from the NE margin of Lake Bafa were undeformed and intruded the amphibolite-facies mica schists and top-to-the-N–NNE fabrics in the so-called augen gneisses, but provided no detailed map or field photographs to illustrate the reported field relations. Thus, the reported field relations and new ages led the authors to suggest that the granites of the southern Menderes Massif and top-to-the-N–NNE amphibolite-facies deformation of the orthogneisses occurred during the Pan-African orogeny. In this interpretation, Alpine deformation of the submassif is confined to greenschist-facies top-to-the-S–SSW shear zones formed during crustal shortening. At almost the same time, Erdoğan & Güngör [86] documented fossil evidence from the metasedimentary sequence exposed at the eastern shore of Lake Bafa; at the same locality from which one of the dated granitic samples of Gessner *et al*. [97] was collected. Carbonates intercalated with pelitic schists close to the granite contact contain thick-shelled bivalve fossils (probably *Megalodon* sp.), and poorly preserved rudist remains up in the succession (see *Fig. 3* in Erdoğan & Güngör [86]), suggesting Late Triassic–Jurassic and Late Cretaceous ages, respectively [86]. This piece of evidence alone indicates that the granite is intrusive into the Upper Triassic to Cretaceous rocks; clearly these fossil findings conflict with the new SIMS ages in this particular part of the southern Menderes Massif. Erdoğan & Güngör [86] concluded that the gneissic granites syn-tectonically intruded (i) the lower parts of the Triassic detrital sequence in the Lake Bafa area and (ii) the Upper Palaeozoic sections of the Kavaklıdere area during regional

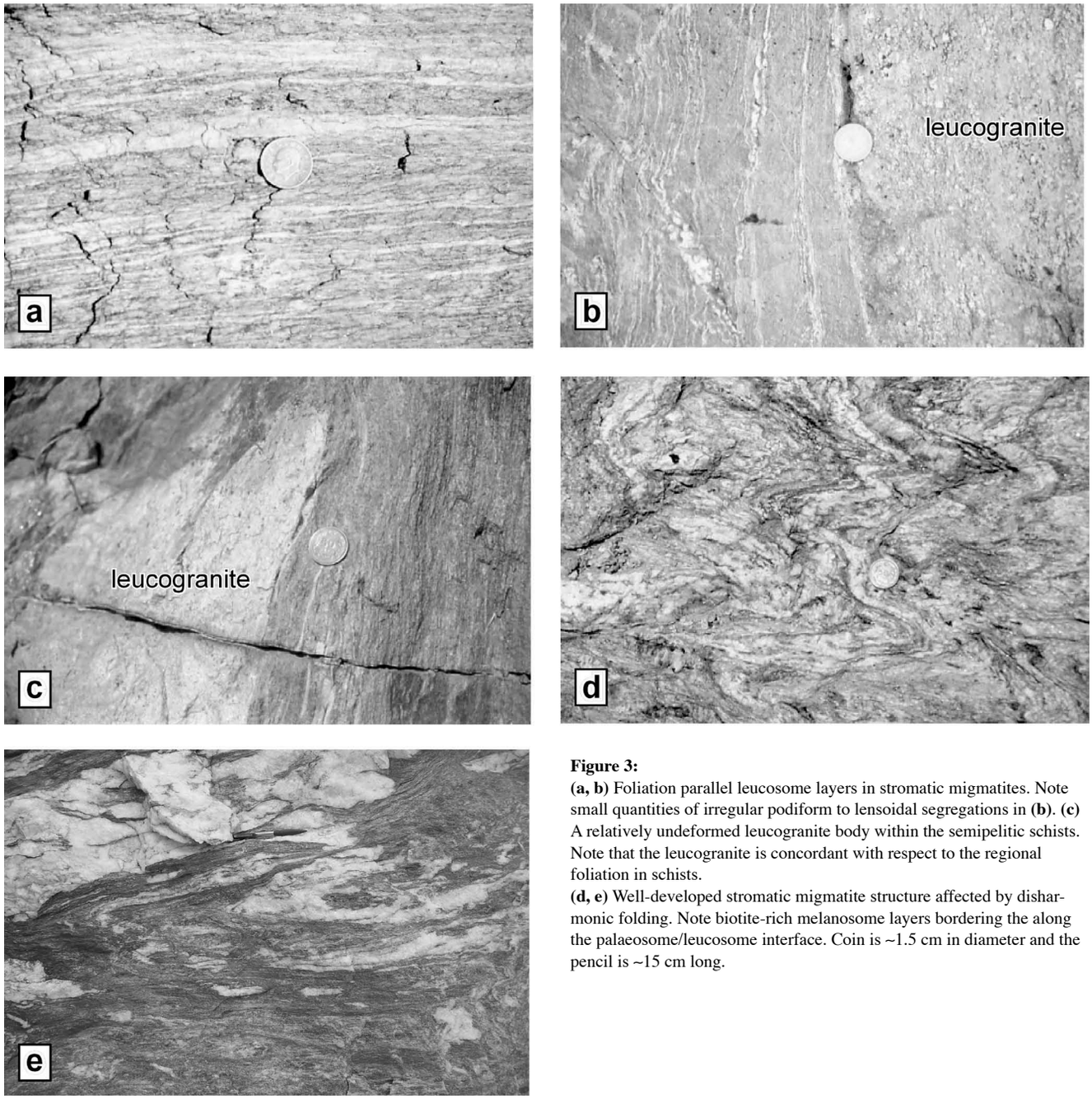

Figure 3:
(a, b) Foliation parallel leucosome layers in stromatic migmatites. Note small quantities of irregular podiform to lensoidal segregations in **(b)**. **(c)** A relatively undeformed leucogranite body within the semipelitic schists. Note that the leucogranite is concordant with respect to the regional foliation in schists.
(d, e) Well-developed stromatic migmatite structure affected by disharmonic folding. Note biotite-rich melanosome layers bordering the along the palaeosome/leucosome interface. Coin is ~1.5 cm in diameter and the pencil is ~15 cm long.

Eocene metamorphism. The close zircon ages between the granites and the adjacent quartz-mica schists (526 to 1984 Ma, Loos & Reischmann [91]) are most probably due to assimilation of the detrital succession by granitic melt and rejuvenation of the country rocks [86].

In addition to these data, recent fieldwork in the southern Menderes Massif around Yatağan (Muğla) showed the existence of two distinct types of granitoid rocks in the so-called '*core*' of the Massif; they differ from one another in intensity of deformation, degree of metamorphism and kinematics: one being the younger (possibly Tertiary) leucogranite and the other being the Precambrian (?) orthogneisses (augen gneisses), where the former is intrusive into the latter and the structurally overlying '*cover*' schists [41]. This present paper documents the results of geochemical analysis of the granitoid rocks exposed in this region.

The boundary relationship between the orthogneisses and the structurally overlying schists has been the subject of a major debate among geoscientists over the last decades. Many workers interpreted this contact as a major unconformity [93, 94, 98–104]. Later, a metaconglomerate unit that crops out in Gökçay valley near the town of Kavaklıdere (Muğla province, Turkey) was interpreted as a basal conglomerate, and therefore used to support the idea of a major unconformity between the orthogneisses and the metasediments [105, 106]. Others, however, argued that there is no unconformity and that the

'*core-cover*' contact is essentially intrusive [77–81, 86], and later became a major extensional shear zone [34–37, 79, 82]. The third and most realistic possibility is that '*orthogneiss-schist*' contact is a major structural discontinuity/shear zone which is referred to as the southern Menderes shear zone (SMSZ; Bozkurt [42]), equivalent to the Selimiye shear zone [95], south Çine shear zone [48], and Kayabükü shear zone [107].

The southern Menderes shear zone is a typical ductile shear zone separating metamorphic rocks of differing metamorphic grades. The footwall is represented largely by orthogneisses while the hanging wall comprises schists (upper schists of Whitney & Bozkurt [75]). The width of the shear zone is variable across the southern submassif from west (Lake Bafa) to east (Yatağan) (Fig. 2). It is suggested here that severely ductilely sheared schists, which are equivalent to the lower schists of Whitney & Bozkurt [75] or metasedimentary rocks of the Çine Nappe of Régnier *et al*. [76], belong tectonically to the southern Menderes shear zone. In other words, the lower and upper boundaries of the southern Menderes shear zone are probably marked by orthogneisses and schists, respectively. Although there is a consensus that the southern Menderes shear zone was associated with Tertiary top-to-the-S–SSW shearing, its origin and nature are highly debated and there are two competing hypotheses. The first considers that the contact is a south-facing, high-angle, greenschist-facies top-to-the-S–SSW extensional shear zone formed during late orogenic Alpine extension in southwestern Turkey [34–37, 43, 41, 44, 48, 50, 69, 75, 82, 89, 108] because there are two different fabrics in this part of the Menderes Massif, one of which is the regional foliation associated with top-to-the-N–NNE shearing during the Eocene main Menderes metamorphism and this is overprinted by low-grade shear bands, indicating a top-to-the-S–SSW shearing [41, 42 and references therein]. Contrary to this view, others argue for a south-facing thrust fault along which the schists (Selimiye nappe of Ring *et al*. [95]) were emplaced onto the granitic rocks (Çine nappe of Ring *et al*. [95]) during greenschist-facies top-to-the-south Alpine nappe stacking in the massif area [45, 76, 92, 95, 97, 109, 110]. This model refutes the presence of top-to-the-N–NNE shearing in the metasediments of the southern submassif although it has been documented well throughout the Menderes Massif. However, the available field, structural, thermochronologic and geochronologic data integrated with *P–T* paths support an extensional origin for the southern Menderes shear zone [42]. The southern Menderes shear zone represents a jump in metamorphic grade on the order of 2 kbar between the hanging-wall and footwall schists, suggesting a metamorphic section of about 7 km thick is absent [76]. The shear zone also correlates closely with major topographic and morphological changes. In contrast to these authors, Erdoğan & Güngör [86] claimed that the contact is intrusive and does not form a major structural discontinuity.

The present paper also utilizes a ternary diagram and fields defined by Henry & Guidotti [111] that uses tourmaline as a petrogenetic indicator in an effort to solve this longstanding tectonostratigraphic problem. This paper also presents the geochemical characteristics (major- and trace-element data) of the granitic rocks in the footwall of the southern Menderes shear zone, interpreting their tectonic environment of emplacement and discussing their geodynamic significance with regard to the tectonometamorphic evolution of southern Menderes Massif. The geochemical data confirm the existence of two distinct granitic rocks in the southern Menderes Massif. Finally, the possible relationship between metamorphism, crustal melting, granite emplacement and orogenic collapse during the evolution and exhumation of the southern Menderes Massif is discussed.

3. Summary of Field Relations, Petrography and Fabric

The hanging wall of the southern Menderes shear zone consists in sequence of: (1) semipelitic (biotite+quartz± muscovite±garnet) and psammitic (quartz+muscovite±biotite) gneisses (lower schists of Whitney & Bozkurt [75]); the semipelites are characterized by the sporadic occurrence of garnet near the contact with the orthogneisses, (2) pelitic schists (garnet+mica, mica+quartz±garnet±chloritoid schists) with carbonate lenses and bands (upper schists of Whitney & Bozkurt [75]), (3) a sequence of metapelites dominated by mica schists and phyllites with dolomitic marble intercalations and (4) a calcareous sequence of marbles with phyllite intercalations (so-called marble-cover) (Fig. 2). All are strongly foliated (S_1), dip southward, and contain shear-sense indicators that record top-to-the-N–NNE simple shear fabrics [37, 43, 75]. Near the granite contact, semipelitic gneisses locally occur as stromatic migmatites characterized by layers of leucocratic granitic material, leucosome or *lit-part-lit* intrusion of granite (Fig. 3). Individual leucosome layers, often discontinuous, are a few centimetres thick and broadly parallel to the foliation in the host rock (Fig. 3a). In phlebitic migmatites at some localities the leucosomes form a random network of vein-like leucocratic material (Fig. 3b) and appear to be segregated locally from their host rocks over a distance of a few millimetres to several centimetres, since the schists (melanosome or restite) at the margin of the leucosome are very dark in colour, having been depleted in leucocratic minerals (Fig. 3a, b). Although the degree of migmatization varies considerably both at outcrop scale and throughout the study area, it is especially well-developed close to the contact. Melanosomes are in most cases poorly developed and indistinguishable from palaeosomes.

The footwall of the southern Menderes shear zone comprises two contrasting types of granitic rocks: older, presumably Precambrian orthogneisses (traditionally known as 'augen gneisses') and younger leucogranites, which occur only along the contact with the structurally overlying metasediments (see *Figure 3* in Bozkurt [41]). The distinction is totally based on contact relations and lithological characteristics (grain size and colour), intensity of deformation, degree of metamorphism, and kinematics. The leucogranite displays local intrusive/cross-

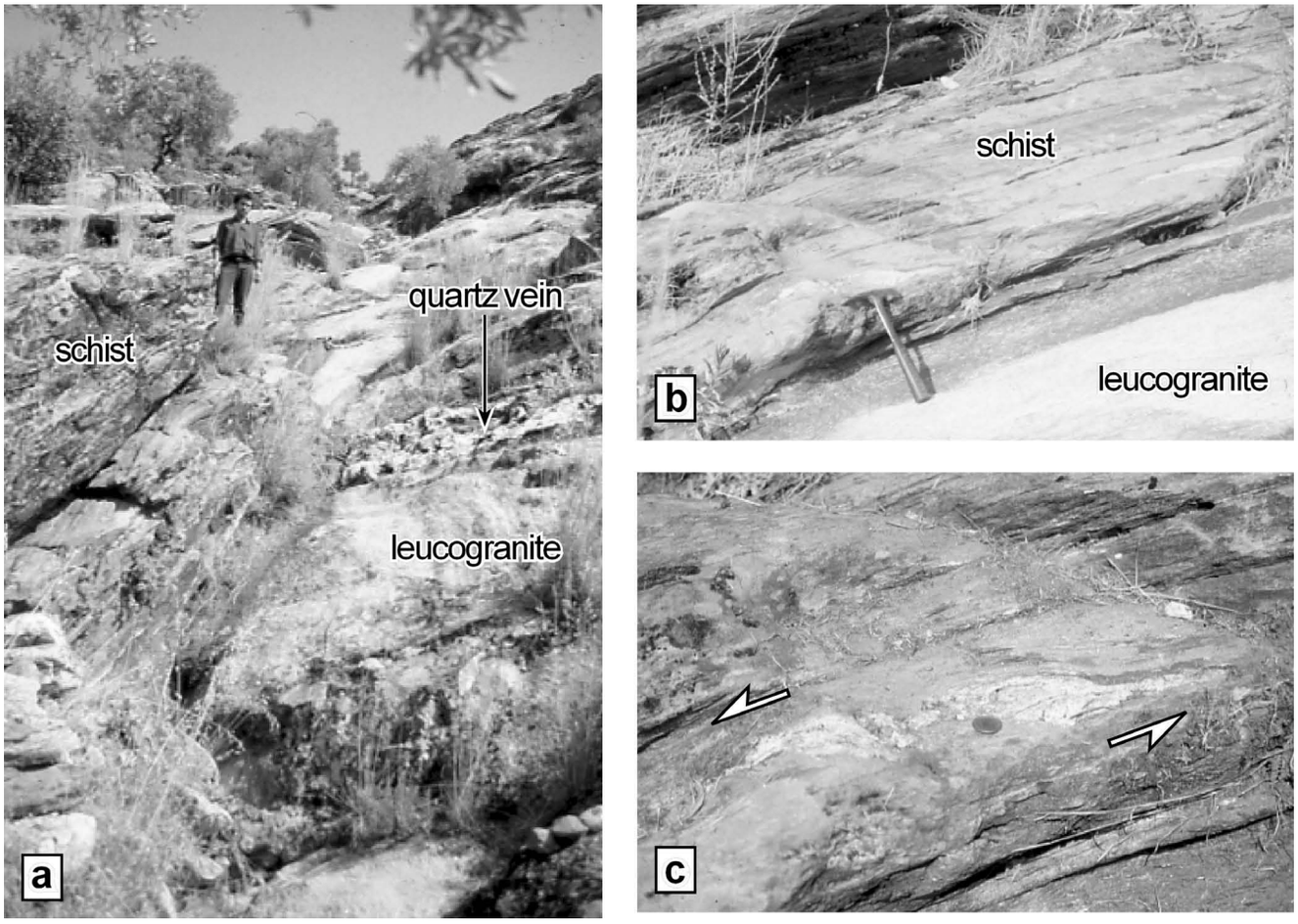

Figure 4: (a) General appearance of the boundary between the leucogranites and the structurally overlying schists in Kayabükü. Man is about 1.70 cm high. **(b)** Close-up view of the same boundary. Note that the boundary is sharp and approximately concordant/parallel to the regional foliation in the schists. Hammer is ~34 cm long. **(c)** Assymmetric, retort-shaped boundinaged granitic vein cutting across the regional foliation in schists at the boundary with leucogranites. The asymmetry of vein indicates a top-to-the-left (down to the south) sense of shear. Coin is ~1.5 cm in diameter.

cutting relationships, not only with the structurally overlying metasediments (garnet-bearing metapelites), but also with the mylonitic orthogneisses.

The orthogneisses, which are abundant and widespread in the southern Menderes Massif, comprise coarse- to very coarse-grained with a range of textural and mineralogical variations, and are characterized by a penetrative mylonitic foliation and associated mineral-stretching lineation. Both fabric elements are defined by micas, elongated and flattened, dynamically recrystallized feldspars and quartz. Large asymmetric rigid feldspar porphyroclasts (with maximum lengths up to 7 cm) with surrounding ductile fine-grained matrix is the most common texture of these rocks. Plagioclases are generally weakly zoned but in many cases display albite twinning. Quartz occurs as anhedral crystals with characteristic undulose extinction. Feldspars are typically intergrown with quartz and occur as large crystals surrounded by a dynamically recrystallized matrix of finer-grained quartz, mica and feldspar, thus defining a typical core-and-mantle microstructure. Biotite and muscovite occur as mica laths that define the mylonitic foliation of the rock; they also occur as inclusions in plagioclase and alkali feldspars. The proportion of muscovite and biotite is variable and differs from one sample to another. Anhedral garnet occurs sporadically. Accessory minerals are apatite, zircon, monazite and opaque phases. The microstructures of deformed micas, quartz and feldspar are consistent with metamorphism and deformation at upper-amphibolite facies conditions (Bozkurt, unpublished data). The orthogneisses display two distinct fabrics with opposite senses of shear: penetrative top-to-the-N–NNE amphibolite-facies structures; and top-to-the-S–SSW greenschist-facies structures superimposed on and proximal to the southern Menderes shear zone.

Most leucogranites are layer-parallel sills/sheets (Fig. 4 and 5a–c), and a few cross-cut the top-to-the-N–NNE regional foliation both in the orthogneisses and metasediments and occur as dykes of variable orientation (Fig. 5d, e). They all occur within the southern Menderes shear zone and do not penetrate/intrude the hanging-wall schists. They are greyish to white, fine-grained equigranular rocks made up of feldspar (K-feldspar and plagioclase), quartz, muscovite and scarce biotite as essential minerals. Tourmaline, zircon, rutile, monazite and opaque phases comprise the accessories.

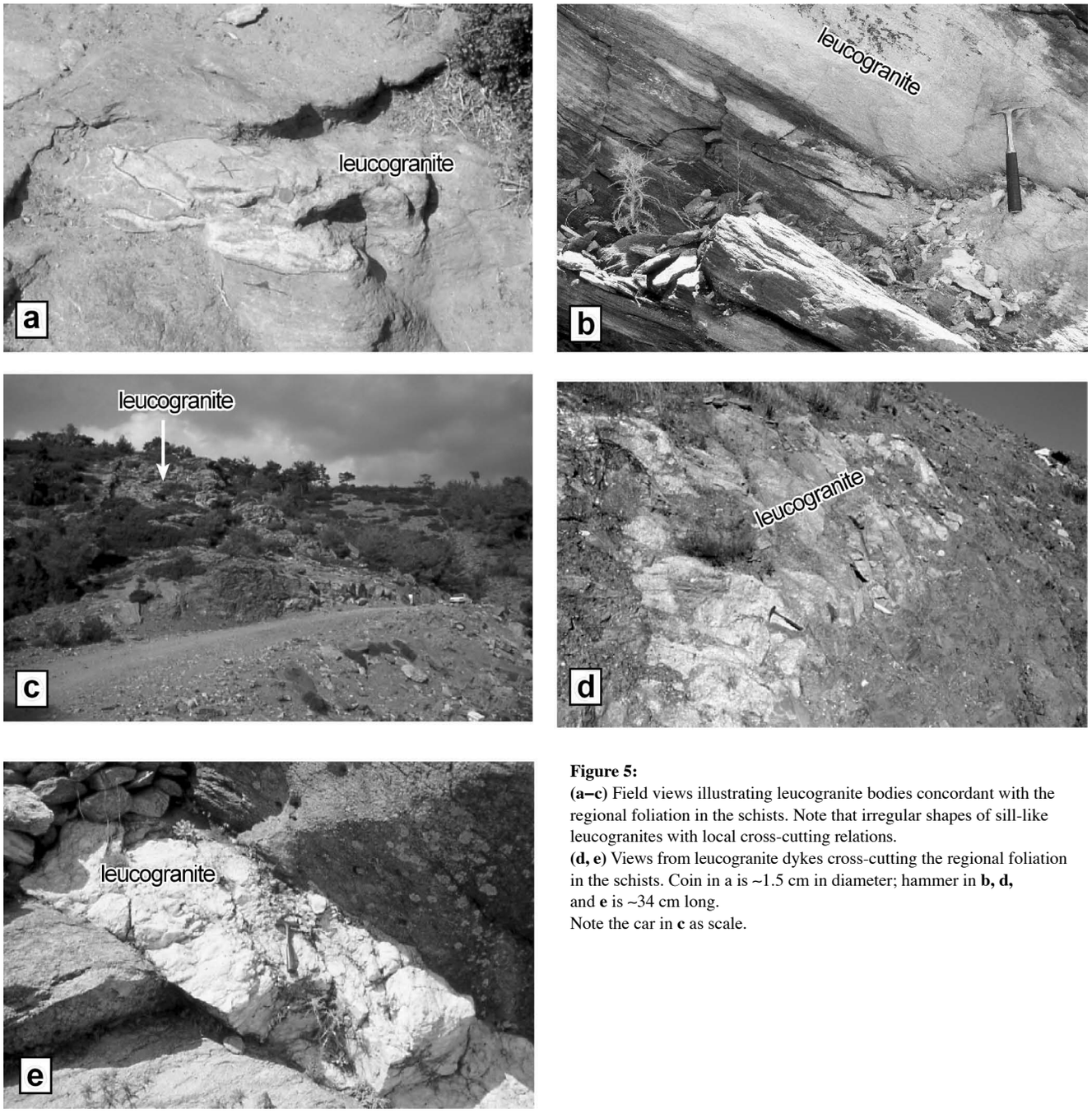

Figure 5:
(a–c) Field views illustrating leucogranite bodies concordant with the regional foliation in the schists. Note that irregular shapes of sill-like leucogranites with local cross-cutting relations.
(d, e) Views from leucogranite dykes cross-cutting the regional foliation in the schists. Coin in a is ~1.5 cm in diameter; hammer in **b, d,** and **e** is ~34 cm long.
Note the car in **c** as scale.

Disseminated (radial clusters or aggregates) tourmaline and quartz-tourmaline nodules form the most diagnostic features of the leucogranites and they are particularly abundant near the contact with the schists. On the basis of field (cross-cutting) relations, petrology and degree of deformation, our field mapping shows the presence of at least two suites/generations of leucogranites: earlier foliation-parallel muscovite+tourmaline (±biotite)-rich leucogranites and later relatively less-deformed muscovite+tourmaline-rich leucogranites. The former were emplaced parallel to the foliation in the metasediments, are mylonitic and display ~E–W-trending planar and ~N–trending linear fabrics. These fabrics are defined by the parallel alignment of micas and elongated quartz grains. The latter are either undeformed or variably deformed – depending on their structural position within the shear zone – and occur at higher structural levels (Fig. 6a–d). Ductile deformation becomes more pronounced in the sill/sheet-like intrusions within the southern Menderes shear zone and is represented locally by the development of typical top-to-the-S–SSW S-C fabrics (Fig. 6b). Within the main body of irregular massive intrusions, local and isolated, top-to-the-S–SSW low-temperature shear zones are also abundant. Leucogranite deformation tends to lack the top-to-the-N–NNE fabrics and usually displays only the top-to-the-S–SSW fabrics (although there are a few very

local observations of top-N–NNE fabrics) in the leucogranites. These observations suggest that most leucogranites post-date the top-to-the-N–NNE deformation. A detailed discussion of the petrography, shear-sense indicators, and microstructures of deformed grains in the metasediments, orthogneisses and leucogranites lies outside scope of this paper and is the subject of a separate paper currently being prepared.

4. Granitoid Geochemistry

4.1. Analytical Methods

Thirty-nine rock samples were powdered in the sample preparation laboratory (Department of Geological Engineering) of Middle East Technical University in Ankara and analysed (Table 1) at Keele University, England, using an ARL 8420 X-ray fluorescence spectrometer, calibrated against both international and internal Keele standards of suitable compositional range, as detailed in Floyd and Castillo [112]. Analytical methods and precision have been described in Winchester *et al*. [113]. A subset of twelve samples were also analysed for rare-earth elements and Cs, Hf, Sc, Ta and U using a PE-Sciex Elan 6000 Inductively-Coupled Plasma Mass Spectrometer (ICP-MS) at Durham University [114].

4.2. Composition of Igneous Suites

Except for a single pelitic gneiss, all the remaining 38 samples were igneous and of broadly granitoid composition. SiO_2 contents in all these rocks exceed 70%, so that all plot (Fig. 7a) in the rhyolite (granite) field on a total alkali-silica (TAS) diagram [115]. Although these rocks are relatively fresh, they were also plotted on a Zr/TiO_2–Nb/Y discriminant diagram [116], which showed a distinct difference of Nb/Y contents between the orthogneisses and the Tertiary leucogranites and a tendency towards lower Zr/TiO_2 in the orthogneisses, which tend to cluster in the rhyodacite/dacite field (Fig. 7b). This result is inconsistent with those of the TAS diagram, suggesting that the orthogneisses have undergone SiO_2 enhancement, possibly during metamorphism.

4.3. Discrimination Between Igneous Suites

The geochemical differences between the leucogranites, orthogneisses and various dyke rocks are elucidated in the following binary plots. A Na_2O-K_2O diagram (Fig. 7c) shows that all the dyke rocks have a distinctive sodic enrichment, such that their compositions approach those of ocean ridge granites. In contrast, the leucogranites and orthogneisses possess K_2O contents typical of continental granites and are essentially calc-alkaline, peraluminous S-type granites.

Harker diagrams hint at some of the distinctions between the Menderes granitoid rock types, even though the range of SiO_2 contents is restricted to between 71% and 80%. Where SiO_2 is plotted against TiO_2, the younger leucogranites are distinguishable from both the orthogneisses and the dyke rocks by their lower TiO_2 contents (Fig. 8a). In contrast, plots of SiO_2 against Al_2O_3, Fe_2O_3(total) and MgO fail to discriminate at all between any of the rock types (Fig. 8b–d); they merely show a general slight negative trend, as might be expected. By contrast, lower CaO and higher Na_2O distinguish the younger leucogranites on CaO-SiO_2 and Na_2O-SiO_2 plots (Fig. 8e, f), and on the latter plot the high Na_2O content of the dyke rocks is quite evident. These sodic dykes are also distinguished on a K_2O-SiO_2 diagram (Fig. 8g), which otherwise fails to distinguish the younger leucogranites from the orthogneisses. Higher P_2O_5, however, does separate the younger leucogranites from the orthogneisses on a P_2O_5-SiO_2 plot (Fig. 8h), as does a plot of Rb against SiO_2 (Fig. 9a). Other trace-element plots against SiO_2, notably Nb-SiO_2, Sr-SiO_2, Sc-SiO_2, Ba-SiO_2 and V-SiO_2 (Fig. 9b–g), failed to discriminate between the rock types at all. Only a Y-SiO_2 plot (Fig. 9e) separated orthogneisses (with higher Y contents) from both the younger leucogranites and the dyke rocks.

Other discriminant diagrams are more informative and indicate differences between the leucogranites and orthogneisses. A simple binary Y-P_2O_5 diagram (Fig. 10a) discriminates between them, as the granite is characterised by distinctly higher P_2O_5 and tends to have lower Y contents. However, good discrimination may also be shown where Nb/Y (distinctly higher in the granite) is plotted against Zr/P_2O_5 (Fig. 10b), or in a SiO_2-TiO_2 binary plot, wherein the leucogranite contains lower TiO_2 (Fig. 8a). Similarly, the discrimination between leucogranite and orthogneiss is pronounced on K_2O versus Na_2O (Fig. 10c) and Ce/Y versus Nb/Y (Fig. 10d) diagrams.

On a rare-earth element (REE) profile normalised against continental crust (Fig. 11a), all the igneous rocks in the complex pattern possess significant negative europium anomalies. However, the leucogranite is distinguished by its more depleted light REE contents relative to the orthogneisses, and so displays a generally rising profile. Among the dyke rocks, there is a separation into two sets – one displaying marked light REE depletion, the others not. A corresponding depletion in Y accompanied light REE depletion; otherwise there was no further match between light REE depletion and (for example) Na enhancement. A multi-element spider diagram normalised against lower crust (Fig. 11b) displays a concave-up profile, but discriminates less clearly between the leucogranite and the orthogneiss, although there is a tendency for the light ion lithophile elements (LILE) to be more enhanced in the leucogranite, and relatively less enhanced in all the dyke rocks.

4.4. Granite Discriminant Plots

On a Nb-Y diagram [117] (Fig. 12a), almost all the samples plot in the volcanic arc and syn-collisional granite field, with just a hint that the compositions of the orthogneisses and leucogranites may be a bit different. This difference becomes plainer on a Rb-(Y+Nb) diagram [117] (Fig. 12b), which shows that, whereas the leucogranites

Table 1: Major and trace element chemistry of granitoid rocks of the Southern Menderes Massif around Yatağan.

Sample	Y3	Y4	Y6	Y7	Y8	Y9	Y10	Y12	Y13	Y20	Y21	Y22	Y23
									Leucogranites				
SiO_2	75,52	75,56	74,35	73,94	75,45	74,79	74,60	74,40	74,87	76,40	74,96	76,30	73,37
TiO_2	0,07	0,10	0,10	0,08	0,09	0,08	0,11	0,09	0,10	0,05	0,06	0,07	0,09
Al_2O_3	13,51	13,89	15,16	14,29	12,66	13,68	13,89	14,25	13,88	12,96	13,35	13,28	14,54
$Fe_2O_3^t$	1,55	0,31	1,54	1,56	1,97	1,37	1,99	1,57	1,99	1,24	0,92	1,26	1,65
MnO	0,02	0,00	0,02	0,01	0,02	0,01	0,04	0,02	0,03	0,01	0,01	0,01	0,03
MgO	0,00	0,00	0,05	0,07	0,07	0,02	0,05	0,02	0,01	0,00	0,05	0,01	0,01
CaO	0,65	0,45	0,49	0,38	0,31	0,38	0,35	0,31	0,30	0,46	0,38	0,37	0,38
Na_2O	3,92	4,57	4,11	3,65	3,48	3,42	3,16	3,42	3,38	3,49	3,91	3,52	3,92
K_2O	4,30	4,96	5,46	5,29	4,55	5,32	5,55	5,54	5,31	5,06	5,07	5,24	5,22
P_2O_5	0,49	0,36	0,35	0,29	0,23	0,26	0,24	0,23	0,23	0,28	0,26	0,28	0,30
LOI	0,57	0,31	0,80	0,61	0,45	0,61	0,61	0,56	0,54	0,40	0,49	0,42	0,60
S	0,001	0,008	0,005	0,003	0,004	0,001	0,001	0,001	0,005	0,000	0,004	0,001	0,001
Total	100,60	100,50	100,45	100,17	99,29	99,93	100,59	100,41	100,64	100,36	99,46	100,76	100,11
Ba ppm	16	98	22	68	47	35	28	124	24	46	123	97	33
Cl	61	198	322	528	1013	159	360	244	543	89	230	366	274
Co	0	0	1	0	0	0	1	0	0	0	2	0	0
Cr	213	176	132	199	213	220	214	190	212	225	179	229	187
Cs	0,00	0,00	13,24	0,00	0,00	0,00	13,68	0,00	0,00	0,00	4,78	0,00	0,00
Cu	8	1	2	1	5	3	6	2	4	5	4	3	2
Ga	22	19	24	21	21	19	20	20	20	18	19	20	21
Hf	0,00	0,00	0,87	0,00	0,00	0,00	1,19	0,00	0,00	0,00	1,43	0,00	0,00
Nb	14,0	4,0	20,0	13,0	11,0	8,0	15,6	8,0	11,0	8,0	13,8	10,0	12,0
Ni	8	8	5	7	8	8	9	8	7	9	7	10	7
Pb	2	6	4	1	0	7	3	12	5	6	10	8	4
Rb	499	247	466	347	320	342	381	352	378	351	291	327	383
Sc	0	0	5	0	0	0	3	0	0	0	5	0	0
Sr	33	41	18	15	10	24	9	15	6	45	66	16	9
Ta	0,00	0,00	3,24	0,00	0,00	0,00	2,01	0,00	0,00	0,00	2,88	0,00	0,00
Th	12,0	4,0	10,8	12,0	9,0	11,0	9,7	11,0	13,0	9,0	7,4	11,0	10,0
U	0,00	0,00	22,82	0,00	0,00	0,00	2,62	0,00	0,00	0,00	20,24	0,00	0,00
V	6	3	7	0	4	8	2	6	1	5	7	2	7
Y	18	17	25	26	24	21	38	24	23	23	22	24	27
Zn	33	13	32	21	38	24	33	34	36	24	22	23	37
Zr	52	53	68	72	65	63	81	70	74	56	71	59	67
La	0,0	0,0	5,3	2,0	1,0	10,0	3,9	8,0	5,0	1,0	1,8	0,0	3,0
Ce	6,0	0,0	13,9	10,0	12,0	7,0	17,3	12,0	9,0	16,0	3,6	2,0	11,0
Pr	–	–	1,85	–	–	–	1,50	–	–	–	0,67	–	–
Nd	12,0	8,0	6,5	10,0	16,0	5,0	5,6	4,0	8,0	13,0	2,6	5,0	19,0
Sm	–	–	2,31	–	–	–	1,93	–	–	–	1,16	–	–
Eu	–	–	0,07	–	–	–	0,05	–	–	–	0,06	–	–
Gd	–	–	2,54	–	–	–	2,39	–	–	–	1,59	–	–
Tb	–	–	0,61	–	–	–	0,57	–	–	–	0,40	–	–
Dy	–	–	3,78	–	–	–	3,80	–	–	–	2,63	–	–
Ho	–	–	0,64	–	–	–	0,77	–	–	–	0,50	–	–
Er	–	–	1,59	–	–	–	2,18	–	–	–	1,34	–	–
Tm	–	–	0,24	–	–	–	0,39	–	–	–	0,22	–	–
Yb	–	–	1,39	–	–	–	2,47	–	–	–	1,33	–	–
Lu	–	–	0,17	–	–	–	0,35	–	–	–	0,18	–	–

plot in the syn-collisional granite field, the orthogneisses plotted immediately adjacent to them – but in the volcanic-arc granite field. Assorted dyke rocks also plotted in the latter field. However, neither of these diagrams allow the recognition of the precise tectonic setting of granitoids and cannot distinguish post-orogenic granitoids from others because on them post-orogenic granites can plot in all the fields except for ocean ridge granites. We therefore utilize a Rb/Sr versus SiO_2 discrimination diagram [118] on which the leucogranites plot within Group II syn-collisional granite field, while orthogneisses plot in the Group III post-collisional granite field (Fig. 12c). However, as these diagrams rely on Rb stability; their significance must be interpreted with care. Rb concentrations might have been depleted in the orthogneisses during deformation and associated metamorphism. By contrast, both sets of granitoid rocks of the southern Menderes Massif cluster in the post-orogenic field (POG) when they are plotted on Al_2O_3 versus SiO_2 diagram of Maniar & Piccoli [119] (Fig. 12d). As this diagram is more reliable since it utilizes relatively immobile major elements, we consider that both sets of granitoid rocks in the southern Menderes Massif were emplaced during late syn- to post-orogenic settings.

5. Tourmaline Chemistry

Henry and Guidotti [111] argued that the complex chemical variability of tourmaline and its relation to coexisting phases might make tourmaline a sensitive indicator of the

Y24	Y25	Y55	Y2	Y19	Y26	Y15	Y16	Y28
					Dykes and Sills			
74,73	74,93	76,26	74,90	76,10	71,89	75,26	76,96	78,55
0,09	0,10	0,04	0,10	0,18	0,31	0,09	0,14	0,11
13,66	13,60	13,06	14,86	14,48	14,99	13,35	12,75	13,41
1,50	1,34	1,08	1,25	1,37	3,00	1,83	0,95	1,23
0,02	0,01	0,01	0,01	0,01	0,03	0,02	0,01	0,01
0,00	0,20	0,21	0,00	0,35	0,59	0,01	0,24	0,21
0,34	0,41	0,55	0,85	0,64	0,59	0,38	0,81	0,85
3,78	3,71	3,32	6,17	5,78	4,60	3,14	5,83	3,92
5,41	5,21	5,23	1,40	0,98	2,57	5,12	0,90	1,59
0,25	0,28	0,40	0,42	0,20	0,21	0,27	0,25	0,15
0,38	0,46	0,47	0,74	0,69	1,22	0,59	0,67	0,25
0,003	0,002	0,001	0,005	0,001	0,004	0,000	0,002	0,005
100,16	100,26	100,64	100,71	100,77	100,00	100,07	99,50	100,27
83	86	257	98	194	337	71	255	212
500	195	81	119	60	84	73	50	108
0	1	0	2	0	3	0	3	3
203	197	191	198	210	229	210	215	214
0,00	7,38	0,00	1,55	0,00	5,98	0,00	1,18	0,64
2	3	5	9	1	10	3	1	6
20	17	21	21	15	17	17	12	17
0,00	0,47	0,00	1,05	0,00	0,24	0,00	1,10	0,65
10,0	13,2	11	17,1	1,0	11,0	8,0	1,9	8,8
8	9	11	7	12	15	8	11	12
1	4	1	17	0	0	6	0	0
331	271	342	132	34	131	337	28	55
0	5	0	4	0	6	0	3	4
19	22	56	152	102	57	49	130	158
0,00	1,65	0,00	5,59	0,00	1,19	0,00	0,31	1,43
11,0	11,0	14,0	13,0	8,0	10,2	12,0	6,8	8,1
0,00	2,63	0,00	8,29	0,00	5,40	0,00	2,68	3,70
9	3	0	4	24	27	0	25	14
29	25	25	20	26	42	27	13	12
25	25	21	33	26	27	39	36	13
62	80	70	75	87	129	76	68	66
3,0	8,5	4,0	3,4	27,0	23,8	6,0	18,1	3,1
13,0	23,2	4,0	8,9	53,0	50,2	18,0	14,7	6,3
	3,05	–	1,30	–	6,51	–	4,83	0,88
19,0	10,8	12,0	4,8	34,0	24,3	21,0	18,0	3,7
–	2,90	–	2,09	–	5,29	–	3,49	1,24
–	0,17	–	0,13	–	0,89	–	0,69	0,24
–	2,38	–	2,47	–	5,27	–	2,75	1,65
–	0,55	–	0,61	–	1,00	–	0,41	0,33
–	3,56	–	3,71	–	6,37	–	1,89	1,94
–	0,73	–	0,62	–	1,33	–	0,33	0,36
–	2,16	–	1,53	–	3,82	–	0,85	0,93
–	0,38	–	0,25	–	0,64	–	0,13	0,15
–	2,48	–	1,45	–	3,98	–	0,92	1,00
–	0,34	–	0,17	–	0,60	–	0,14	0,16

local environment in which it formed, especially considering its mechanical and chemical stability. From over 60 published sources they plotted tourmaline compositions from various rock types on ternary diagrams and then defined fields for tourmalines from different rock types. As noted by Henry and Guidotti, if their fields are valid, "then knowledge of the composition of a tourmaline from an unknown source should permit a reasonable evaluation of the original rock type in which it formed" (p. 4). Since the publication of their cogent paper, many other workers have used the Henry and Guidotti classification scheme to refine understanding of or elucidate environments of formation [e.g., 120–128]. The reader is referred to Henry & Guidotti [111] for a detailed explanation of the advantages and potential disadvantages of their diagrams.

5.1. Material and Methods

Tourmaline-bearing rocks, including tourmaline-rich pebbles from the Gökçay metaconglomerate, were collected from a variety of environments in 11 different sampling areas in the southern and central parts of the Menderes Massif. The modes of tourmaline occurrence in the Menderes Massif have been discussed elsewhere [129], and more detailed studies of stratiform tourmalinites [cf. 130], other massive quartz-tourmaline rocks and quartz-tourmaline nodules have been undertaken [83–85]. Electron-microprobe analyses of tourmalines in these rocks were performed on a Cameca SX-50 instrument in the laboratories of the Geological Survey of Canada. Accelerating voltage was 15 kV, beam size was about 5 μm, and beam current was 10 nÅ with a counting time of 20 seconds for Na, K, Mg, Fe, F, Cl, Si and Mn, and 30 nÅ with a counting time of 30 seconds for the other elements. Natural minerals, synthetic equivalents and pure metals were used as standards. Data reduction was conducted according to the methods of Pouchou & Pichoir [131].

Structural formulae for tourmaline were calculated on the basis of 29 oxygen atoms and with the assumption that B is stoichiometric. Formulae with Si in excess of 6 atoms per formula unit were normalized to 6 atoms.

5.2. Results

Eighty-six tourmaline analyses from the Menderes Massif were plotted on the Al-Fe(tot)50Al50 -Mg50Al50 diagram of Henry & Guidotti [111]. The tourmalines analysed in this study are all in the schorl-dravite compositional series, with the exception of the Sarıgöl tourmalinites (locality outside of the area shown in Fig. 2) that fall just into the uvite field due to their high CaO contents (Mittwede, unpublished data).

The petrogenetic environments for each sample of tourmaline-rich rock from the Menderes Massif are known except for the tourmaline-rich pebble from the Gökçay metaconglomerate. For example, all the tourmaline rocks plotted in Fig. 13a are stratiform (sediment-hosted) tourmalinites, except for the Labranda massive quartz-tourmaline rock that occurs as lenses within the leucocratic metagranite unit that extends east from Lake Bafa to near Madran Mountain [79]. These lenses, measuring up to 6 m by 2 m, strike approximately N10ºE, are vertical or steeply dipping to the southeast; and

Table 1: Continued.

Sample	Y1	Y29	Y30	Y31	Y32	Y33	Y34	Y35	Y36	Y37
								Orthogneisses		
SiO_2	74,83	73,62	73,62	73,34	75,85	75,30	79,07	76,73	77,03	75,34
TiO_2	0,14	0,25	0,25	0,15	0,13	0,15	0,18	0,19	0,12	0,17
Al_2O_3	13,52	14,29	13,94	14,59	13,19	13,12	11,46	12,90	12,71	13,53
$Fe_2O_3^T$	1,71	1,85	1,77	1,72	1,36	1,65	1,58	1,65	1,27	1,37
MnO	0,03	0,02	0,02	0,03	0,03	0,03	0,02	0,03	0,02	0,03
MgO	0,08	0,28	0,21	0,13	0,04	0,08	0,17	0,17	0,05	0,10
CaO	0,64	1,12	1,16	0,69	0,68	0,60	1,02	0,99	0,52	0,73
Na_2O	3,13	3,06	3,19	3,34	3,32	3,10	2,61	3,02	2,84	3,29
K_2O	5,42	5,32	5,23	5,80	5,20	5,20	3,87	4,06	5,43	5,16
P_2O_5	0,19	0,21	0,21	0,18	0,17	0,16	0,16	0,15	0,14	0,16
LOI	0,42	0,51	0,44	0,62	0,36	0,50	0,35	0,61	0,43	0,39
S	0,002	0,008	0,002	0,000	0,001	0,001	0,000	0,022	0,000	0,001
Total	100,12	100,52	100,05	100,58	100,33	99,88	100,50	100,52	100,55	100,27
Ba ppm	123	421	380	134	126	111	300	236	120	156
Cl	126	162	137	104	108	462	158	570	235	398
Co	0	0	0	0	1	0	0	0	1	0
Cr	225	237	225	189	218	246	283	204	240	189
Cs	0,00	0,00	0,00	0,00	6,26	0,00	0,00	0,00	4,64	0,00
Cu	3	4	6	4	5	3	6	3	3	6
Ga	18	17	14	19	14	16	12	17	13	15
Hf	0,00	0,00	0,00	0,00	0,24	0,00	0,00	0,00	0,32	0,00
Nb	7,0	8,0	7,0	7,0	8,4	6,0	6,0	6,0	7,1	6
Ni	10	10	8	8	8	9	11	8	9	7
Pb	9	19	16	17	18	13	13	9	18	14
Rb	258	201	192	222	199	205	149	176	197	191
Sc	0	0	0	0	4	0	0	0	3	0
Sr	32	74	76	34	35	37	61	54	42	47
Ta	0,00	0,00	0,00	0,00	0,99	0,00	0,00	0,00	0,77	0,00
Th	10,0	16,0	12,0	14,0	10,2	12,0	12,0	14,0	10,3	11,0
U	0,00	0,00	0,00	0,00	5,53	0,00	0,00	0,00	4,50	0,00
V	6	11	11	6	8	8	22	18	5	5
Y	35	51	52	38	40	33	47	36	25	37
Zn	29	33	35	27	25	25	28	27	27	28
Zr	83	123	117	109	81	92	103	107	87	95
La	11,0	29,0	19,0	7,0	10,5	8,0	16,0	8,0	9,7	11,0
Ce	37,0	55,0	48,0	35,0	24,6	12,0	33,0	32,0	27,5	32,0
Pr	–	–	–	–	3,14	–	–	–	2,98	–
Nd	20,0	26,0	24,0	11,0	11,5	6,0	20,0	31,0	10,7	17,0
Sm	–	–	–	–	3,25	–	–	–	2,83	–
Eu	–	–	–	–	0,26	–	–	–	0,23	–
Gd	–	–	–	–	3,68	–	–	–	2,76	–
Tb	–	–	–	–	0,83	–	–	–	0,59	–
Dy	–	–	–	–	5,69	–	–	–	3,94	–
Ho	–	–	–	–	1,25	–	–	–	0,83	–
Er	–	–	–	–	3,79	–	–	–	2,56	–
Tm	–	–	–	–	0,68	–	–	–	0,47	–
Yb	–	–	–	–	4,47	–	–	–	3,17	–
Lu	–	–	–	–	0,68	–	–	–	0,50	–

formed as metasomatic features in the granitic host within zones of weakness (pull-apart zones) that developed during an episode of extension [83]. The sampled tourmaline vein at the Irmadan locality is hosted by quartz-muscovite schist, while the tourmaline vein from Lake Bafa (specifically, from İkizceler Island [sometimes peninsula], near the north-central shore of the lake) is hosted by leucogranite. All the tourmalines plotted on Fig. 13b have typical magmatic compositions, and are either from quartz-tourmaline nodules that occur in leucogranite at various localities (including Labranda, Irmadan,

Y38	Y39	Y40	Y41	Y42	Y43	Y5 Pelite
74,06	77,21	76,36	74,40	74,35	75,37	47,97
0,15	0,11	0,10	0,16	0,19	0,15	2,12
14,31	12,34	13,00	13,54	13,88	12,79	25,15
1,65	1,32	1,46	1,92	1,80	1,69	6,24
0,03	0,02	0,03	0,03	0,03	0,04	0,04
0,12	0,04	0,06	0,14	0,14	0,11	1,97
0,73	0,58	0,57		0,68	0,63	4,76
3,30	2,84	2,89	3,19	3,08	3,24	0,92
5,52	5,21	5,51	5,01	5,31	4,87	5,66
0,15	0,13	0,16	0,20	0,20	0,17	0,28
0,57	0,27	0,42	0,74	0,62	0,47	5,41
0,001	0,002	0,000	0,002	0,001	0,000	0,001
100,57	100,07	100,55	99,94	100,29	99,52	100,51
148	134	162	139	128	115	645
368	153	280	336	239	303	94
0	1	0	0	0	1	0
214	349	243	208	206	238	241
0,00	5,43	0,00	0,00	0,00	10,70	0,00
4	8	3	3	3	5	33
18	14	13	18	19	18	35
0,00	0,18	0,00	0,00	0,00	0,14	0,00
7	6,5	4	9	9	10	65
7	16	9	9	8	11	74
14	17	16	11	15	14	20
215	196	228	251	253	238	207
0	4	0	0	0	4	0
47	36	40	33	37	31	380
0,00	0,66	0,00	0,00	0,00	1,45	0,00
12,0	9,4	11,0	15,0	12,0	11,4	23,0
0,00	7,36	0,00	0,00	0,00	1,86	0,00
4	11	5	14	2	12	226
37	27	39	37	39	37	61
26	21	25	36	28	28	104
105	71	79	98	101	85	462
7,0	9,3	14,0	10,0	10,0	9,2	64,0
33,0	21,0	33,0	32,0	28,0	28,9	156,0
–	2,78	–	–	–	2,84	–
22,0	9,8	17,0	20,0	20,0	10,0	67,0
–	2,49	–	–	–	2,71	–
–	0,23	–	–	–	0,23	–
–	2,48	–	–	–	2,99	–
–	0,54	–	–	–	0,73	–
–	3,79	–	–	–	5,28	–
–	0,85	–	–	–	1,18	–
–	2,69	–	–	–	3,67	–
–	0,50	–	–	–	0,66	–
–	3,40	–	–	–	4,19	–
–	0,53	–	–	–	0,64	–

İsler-Kisir and Sakarkaya), or are tourmalines disseminated in that unit at the Labranda and Irmadan localities [83].

As is obvious from these plots, the granite-hosted tourmalines plot near the schorl end-member on this ternary diagram (Fig. 13b), and mainly in field 2 (Li-poor granitoids) of Henry & Guidotti [111]. Conversely, the sediment-hosted tourmalines are intermediate in the schorl-dravite series (i.e., more Mg-rich), and plot in fields 4, 5 and 6 of Henry & Guidotti [111], those mainly for metapelites and metapsammites (Fig. 13a). Of primary importance to this discussion is the location in this ternary diagram of the tourmaline-rich pebble from the Gökçay metaconglomerate which yielded tourmaline compositions intermediate in the schorl-dravite series (Table 2, Fig. 13a). These compositions cluster with sediment-hosted tourmalinites, *not* with those that are granite-hosted.

6. Discussion

The southern Menderes Massif comprises two distinct rock units juxtaposed along a regional-scale shear zone – the southern Menderes shear zone. Below the shear zone lie granitoid orthogneisses while metasediments form the hanging wall. The shear zone is characterized by progressive overprinting of amphibolite-facies top-to-the-N–NNE fabrics by greenschist-facies top-to-the-S–SSW mylonitic fabrics which grade locally into breccia and cataclasites. Both the granitoid orthogneisses and the metasediments are intruded by younger, possibly Tertiary, leucocratic metagranites. Rocks in the hanging wall have yielded Eocene (35±4 Ma; Satır & Friedrichsen [94]) cooling ages whereas top-to-the-N–NNE fabrics in the high-grade orthogneisses exhumed in the footwall have yielded an age of 36±2 Ma (Ar-Ar mica ages; Lips *et al.* [48]). The geochemical characteristics of the two types of granitoids are distinct and the differences may reflect differing tectonic settings of emplacement. They indicate that the granitoid rocks of the southern Menderes Massif have compositional characteristics typical of late syn- to post-collisional tectonic setting. However, the compositions of the younger rocks may equally reflect the composition of the lower crustal material that was being melted at a time of local extension.

The following sections concentrate mainly on the tectonic significance of leucogranite and tourmaline compositions from the granites and Gökçay conglomerate. The orthogneisses lie outside the scope of this paper, but we include a brief synopsis of our views on these rocks.

6.1. Leucogranites

Within the southern Menderes shear zone abundant kinematic indicators supply evidence for two distinct phases of deformation: a top-to-the-N–NNE compressional and an overprinting top-to-the-S–SSW extensional deformation. Diffuse networks of leucosomes and sheet-like (sill) veins and dykes of leucogranite bodies, occurring ubiquitously within the immediate footwall of the southern Menderes shear zone from Lake Bafa to Yatağan, are mainly concordant, but rarely discordant with the regional foliation in the metasediments.

The presence of both deformed and slightly deformed to undeformed leucogranites suggests heteregenous and polyphase

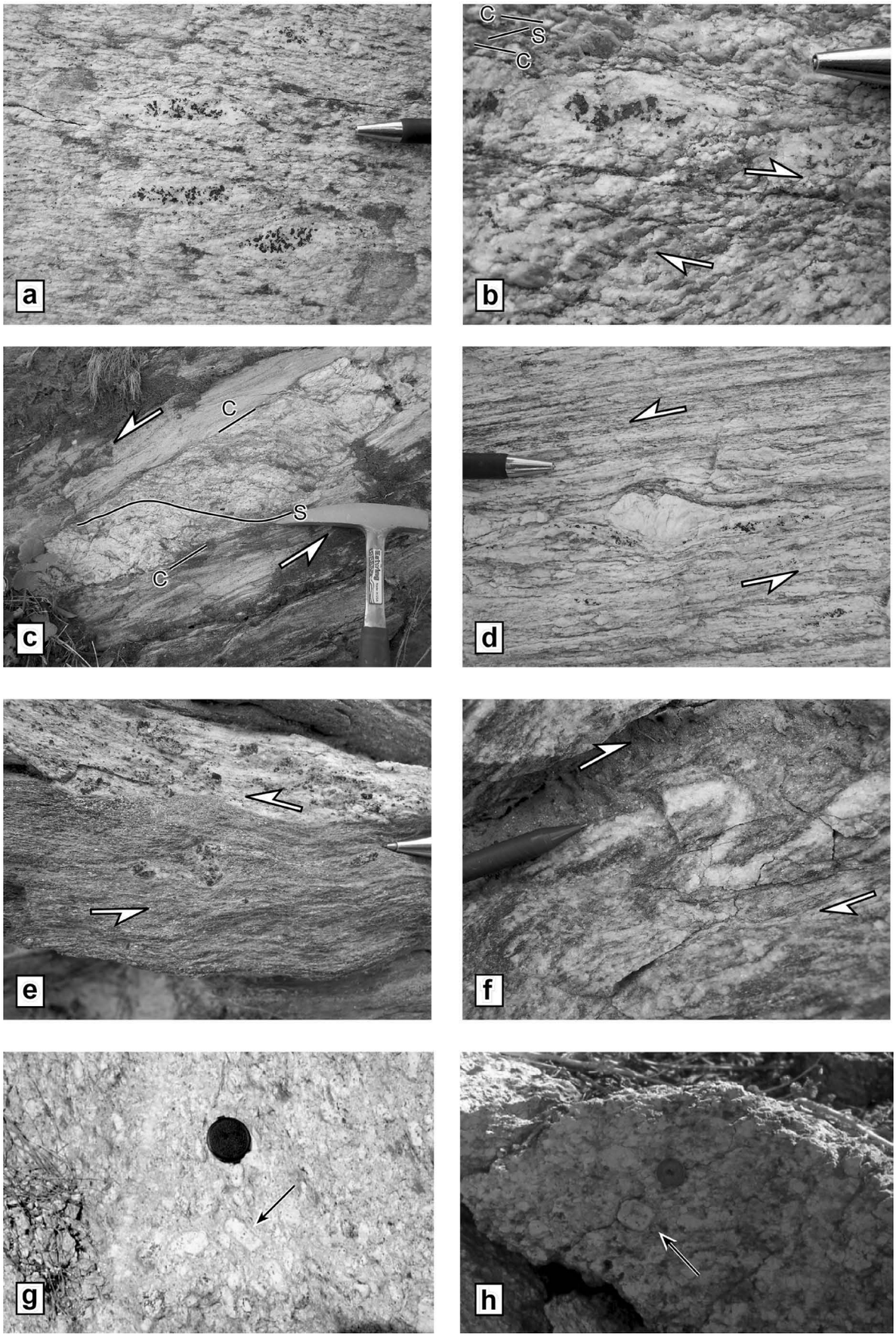
a
C
S
C
b
C
S
C
c
d
e
f
g
h

Figure 6: Field photographs showing various kinematic indicators formed during the deformation of leucogranites in the rocks of the southern Menderes Massif. **(a)** appearance of deformed quartz-tourmaline nodules. Note how nodules are and elongated and flattened in the plane of foliation. **(b)** S-C fabrics developed within the lower schists. The discrete C-surfaces dip gently towards south while S planes are obliquely oriented and dip to the north. Both the C- and S-surfaces are defined by thin seams of muscovite and elongated quartz grains. **(c)** A close up view of a sill-like leucogranite body concordant with the regional foliation in the schists. Note that the contact between leucogranite and schists acted as a shear surface (C-surface) while the leucogranite body posses a well-developed S-foliation. The S-foliation is defined by thin seams of muscovite and elongated quartz-feldspar grains. Please note how S-surfaces bent and curve into parallelism with the main foliation (C-surface). **(d)** Large, rigid asymmetric rigid σ-type feldspar porphyroclast in the intensely deformed leucogranites. The asymmetry of recrystallized tails and stair-stepping geometry is pronounced. All kinematic indicators in **(a–d)** suggest a top-to-the-S–SSW sense of shear in the field; **(e)** A quartz-feldspar-torumaline leucosome flattened and elongated in the plane of regional foliation in the schists. Note that the leucosome is folded into an S-shape asymmetric structure. **(f)** A close-up view from an asymmetric intrafolial fold in the migmatites adjacent to a leucogranite body. Note the thickenning in the hinges. The foliation is defined by flattened/elongated feldspar-quartz rich domains and micas. The flattened/elongated feldspar porphyroclats in the plane of foliation is consistent with, at least, upper amphibolite facies deformation. The geometry of the fold in **(e, f)** is consistent with top-to-the-N–NNE shearing. **(g, h)** Field views of slightly deformed leucogranite without any recognizable fabric. Note the euhedral habit of the feldspar porphyroclasts (arrowed). The pencil is about 13 cm long and the head of the hammer is about 20 cm. The diameters of lens cap and coin are about 5.8 cm and 1.5 cm, respectively.

intrusion. Using cross-cutting relationships and degree of deformation, our mapping shows the presence of at least two distinct phases of leucogranite generation: (i) an older generations of mylonitic, foliated muscovite+tourmaline (± biotite) leucogranites concordant with foliation in the schists (Fig. 4 and 5a–c); some are deformed into asymmetric boudins (Fig. 4c) and display local S-C fabrics (Fig. 6b); (ii) a younger generation represented mostly by muscovite-tourmaline leucogranites which are either undeformed or variably deformed depending on their structural position within the southern Menderes shear zone. They are usually dykelike and crosscut the foliations (Fig. 5d, e) and, locally, the earlier generation of leucogranites. The deformed leucogranites display kinematic indicators consistent with top-to-the-S–SSW (Fig. 6a–d), down-dip sense of shearing while there are rare occurrences of top-to-the-N–NNE (Fig. 6e, f), up-dip sense of shearing.

Ubiquitous foliated leucogranites and top-to-the-S–SSW S-C fabrics (Fig. 6b) suggest that the crust was actively deforming during leucogranite emplacement and implies a continuum of deformation subsequent to their emplacement; this implies both spatial and temporal relationships between extensional shear zone deformation and leucogranite emplacement. The scarce top-to-the-N–NNE fabrics in the leucogranites (Fig. 6e, f) indicate that some relatively early leucogranitic bodies underwent contractional deformation prior to the onset of extension. The occurrence of less-deformed leucogranites with locally preserved magmatic textures (Fig. 6g, h) indicate that melt migration was synkinematic and emplacement occurred during late increments of, or after cessation of, ductile deformation. In conclusion, these

Table 2: Partial analyses of tourmaline cores from a tourmaline-rich pebble, Gökçay metaconglomerate.

Sample	OC93/6-1-51c	OC93/6-1-52c
SiO_2	36.57	36.90
TiO_2	0.52	0.43
Al_2O_3	32.94	31.37
$Fe_2O_3^T$	9.16	10.63
MnO	0.00	0.00
MgO	5.06	4.81
ZnO	0.04	0.00
CaO	0.23	0.20
Na_2O	1.91	2.10
K_2O	0.04	0.05
F	0.00	0.05
$0=F_2$	0.00	0.02
Total	86.47	86.56
B	3.000	3.000
Si	5.993	6.000
Al(t)	0.007	0.000
Al(z)	6.000	6.000
Al(y)	0.355	0.012
Ti	0.064	0.052
Fe^{2+}	1.255	1.446
Mn	0.000	0.000
Mg	1.235	1.446
Zn	0.005	0.000
Y site	2.914	2.676
Ca	0.041	0.034
Na	0.608	0.662
K	0.008	0.010
X site	0.657	0.706
F	0.000	0.028
Lu		

observations are consistent with a model that melt generation, emplacement and deformation were all synchronous and that strain localization in the southern Menderes shear zone is related to the presence of leucogranites. We therefore think that the distribution, field relations and geometric characteristics of the leucogranites and their deformation are controlled by heterogeneous deformation within the first top-to-N–NNE compressional (latest increments), then top-to-the-S–SSW extensional deformation along the southern Menderes shear zone, which was also used as a major pathway for magma.

The accumulation of leucogranites at high structural levels in the immediate footwall of the SMSZ suggest that leucogranite melt migrated upward through the crust along mechanically weak planes (represented by foliation planes in the metasediments) and that the upward migration of leucogranitic melt may have been driven by motion along the southern Menderes shear zone. The apparent lack of contact metamorphism around most of the small leucogranite bodies

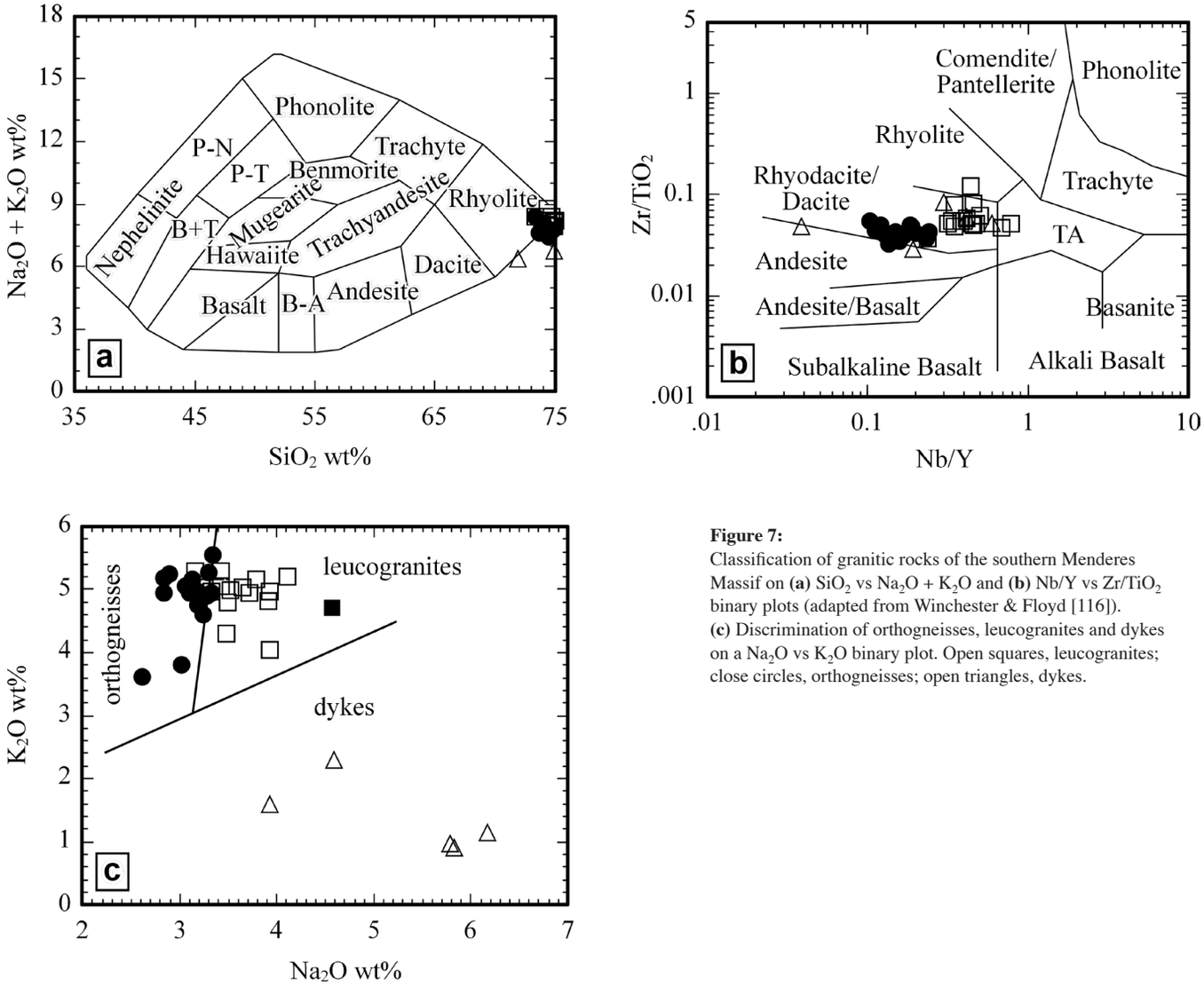

Figure 7:
Classification of granitic rocks of the southern Menderes Massif on **(a)** SiO_2 vs $Na_2O + K_2O$ and **(b)** Nb/Y vs Zr/TiO_2 binary plots (adapted from Winchester & Floyd [116]). **(c)** Discrimination of orthogneisses, leucogranites and dykes on a Na_2O vs K_2O binary plot. Open squares, leucogranites; close circles, orthogneisses; open triangles, dykes.

suggests that temperatures of the host rock were very high. The hot rocks thus must have allowed some amount of melt to migrate upward to high structural levels *without* crystallizing to form leucogranite bodies intrusive into schists with local contact-metamorphic assemblages [80, 81, 88].

The chemistries of the southern Menderes leucogranites in Yatağan area are typical of collisional tourmaline leucogranites (cf. Nabelek & Liu [8]), with low concentrations (<1% wt) of CaO, MgO and FeO and high concentrations of TiO_2 (>0.06% wt) (Table 1). The major- and trace-element compositions of the leucogranites are consistent with a metasedimentary source which was undergoing active metamorphism and deformation during magma genesis, ascent and emplacement into the shallower portions of the source rocks. The abundance of muscovite and tourmaline favours muscovite-dehydration melting of metasediments (pelites) as the dominant mechanism for melt production; this includes breakdown of tourmaline and explains the characteristics of muscovite-tourmaline leucogranites, including the concentration of boron (cf. Wilke *et al*. [132]).

The field relations, structural data and abundance of leucogranites within the southern Menderes shear zone suggest that the shear zone is integral to metamorphism and to leucogranite magma generation, ascent and emplacement. But it is not yet clear if this occurred during the top-to-the-N–NNE compressional or the top-to-the-S–SSW extensional deformation along the southern Menderes shear zone because, while the chemistry of the leucogranites is consistent with a collisional tectonic setting (Fig. 12) their deformation mainly occurred in an extensional shear zone. Similarly, discrimination diagrams for the leucogranites indicate both syn-collisional and post-collisional tectonic settings. The structural aspects of the leucogranites suggest that both phases of deformation along the southern Menderes shear zone may have contributed to melt generation and subsequent emplacement during the whole history of the southern Menderes Massif; this confirms the role of both compressional and extensional deformation.

The preferred orientation of the leucogranites with respect to the regional foliation and their distribution together with occurrences of local migmatites and top-to-the-N–NNE fabrics indicates that the leucogranites were, in part, generated by *in-situ* melting of high-grade metasediments during top-to-the-N–NNE ductile compressional deformation within lower parts of the crust

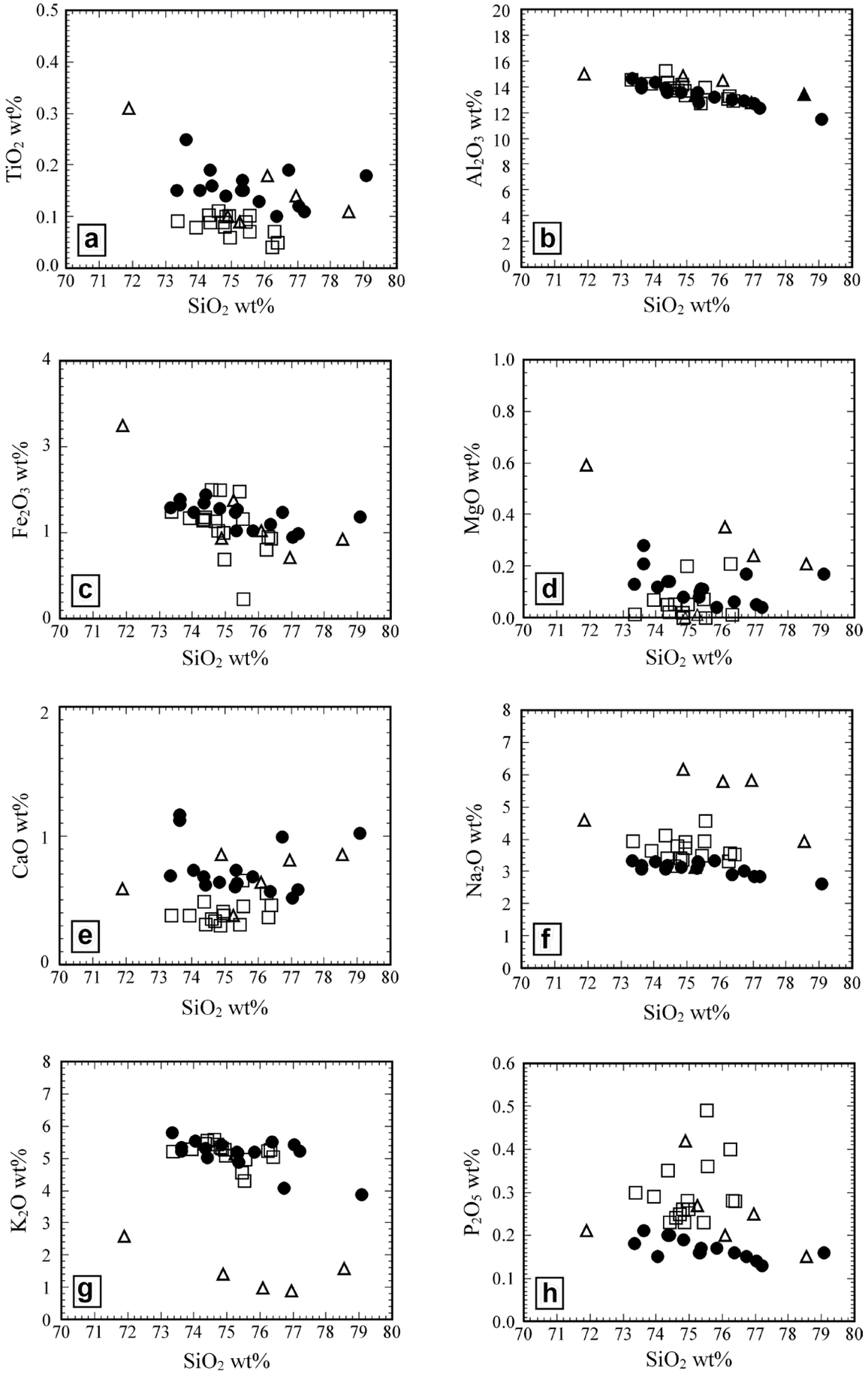

Figure 8:
Variation between major oxides (TiO_2, Al_2O_3, Fe_2O_3, MgO, CaO, Na_2O, K_2O and P_2O_5) and SiO_2. Open squares, leucogranites; close circles, orthogneisses; open triangles, dykes.

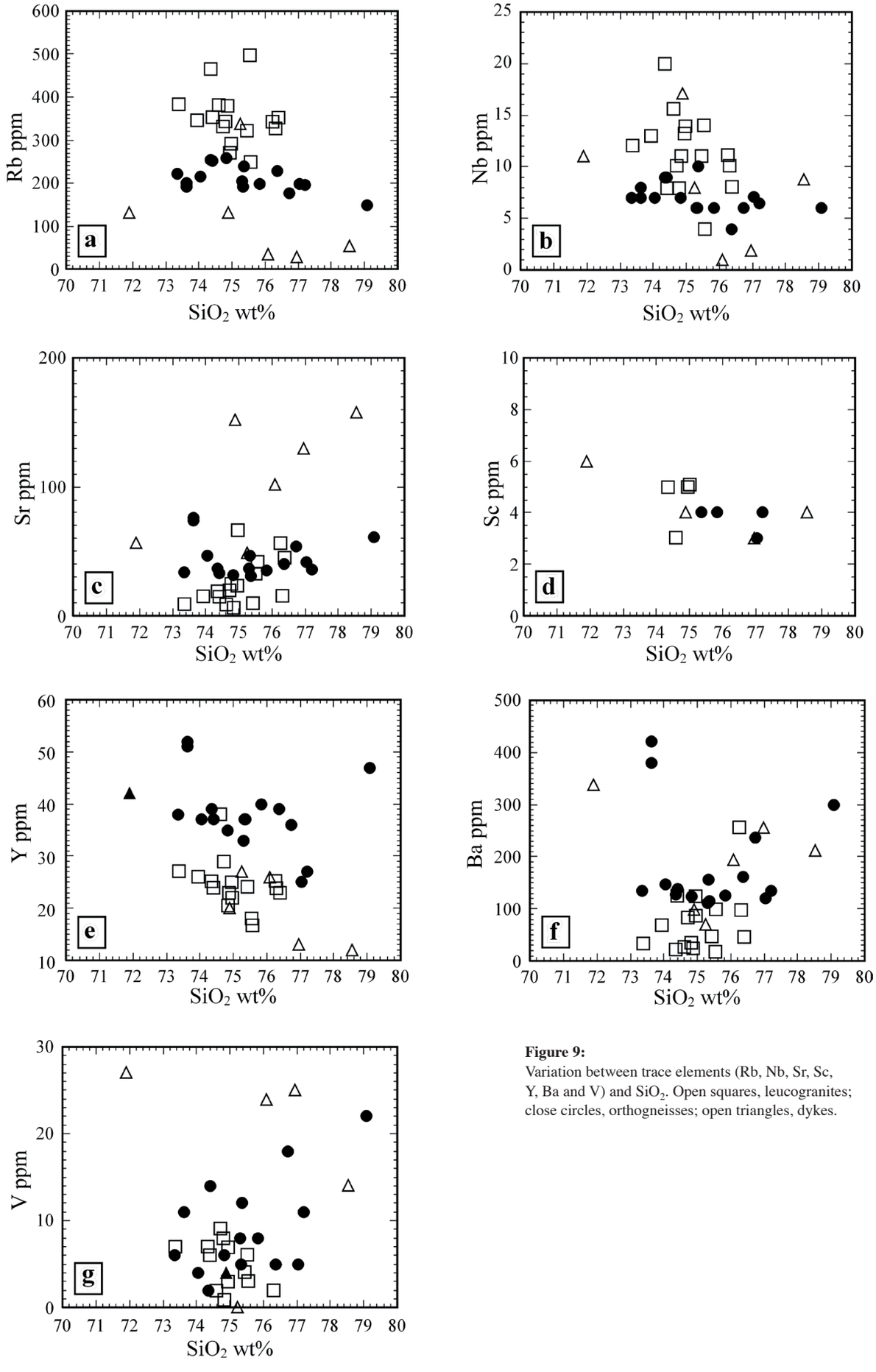

Figure 9:
Variation between trace elements (Rb, Nb, Sr, Sc, Y, Ba and V) and SiO_2. Open squares, leucogranites; close circles, orthogneisses; open triangles, dykes.

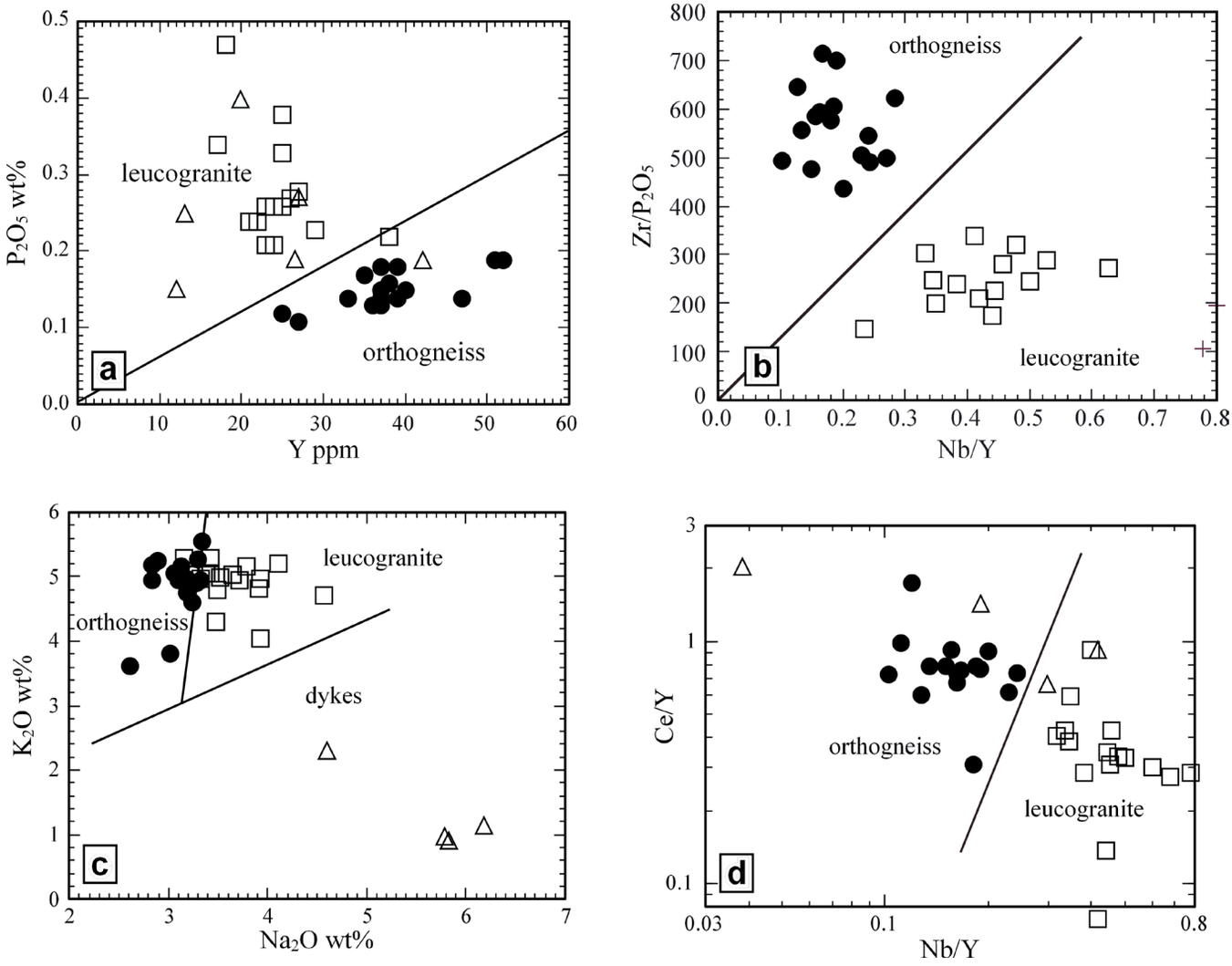

Figure 10: Discrimination of orthogneisses, leucogranites and dykes on **(a)** Y vs P2O2, **(b)** Nb/Y vs Zr/P2O5; **(c)** Na2O vs K2O and **(d)** Nb/Y vs Ce/Y binary plots. Open squares, leucogranites; close circles, orthogneisses; open triangles, dykes.

and that regional deformation played a major role in providing pathways for melt migration and possibly emplacement. We propose that this melt generation occurred during the latest (waning) stages of the main Menderes metamorphism and associated top-N–NNE deformation. Metamorphism proceeded until the onset of leucogranite generation, which marked the latest stages of deformation of the host rocks. Following magma generation, melt migrated from source regions into dilatant portions of the southern Menderes shear zone, which was possibly undergoing compressional deformation (cf. Brown & Solar [133]). We therefore speculate that shear heating along the top-N–NNE southern Menderes shear zone could explain the generation of some of leucogranites in the SMM as in other examples worldwide [e.g., 5, 8, 134–138]. This model could also explain the inverted metamorphic sequence documented in the central Menderes Massif [38, 71–73]. Thus, following partial melting in the crustal-scale southern Menderes shear zone, leucogranitic melts migrated along the shear-zone system to higher structural levels in the crust due to a pressure gradient generated by buoyancy and tectonic stresses. In this model, leucogranite magmatism was partly syn-kinematic with crustal thickening, although contact metamorphic aureoles were superimposed on shallower, earlier-deformed parts of the metasediments by growing plutons (cf. Brown & Solar [133], Solar *et al*. [139]; Schneider *et al*. [140]; Solar & Brown [141]).

As a result of melt generation, shear stress in the southern Menderes shear zone dropped dramatically, possibly resulting in cessation of the thrust-related top-to-the-N–NNE deformation. The presence and upward migration of leucogranitic melt may have affected the rheology of rocks and induced strain localization along the shear zone, as in other examples worldwide [e.g., 1, 142–145]. The leucocratic melts weakened the formerly sheared rocks and facilitated rapid crustal extension, exhumation and tectonic unroofing. The emplacement of leucogranites thus may have promoted the reactivation of the southern Menderes shear zone as an extensional feature. If so, the top-to-the-S–SSW shearing then became localized at the contact between the orthogneisses and metasediments allowing younger leucogranites to cut the shear zone fabrics formed at depth. The continuum of top-to-the-

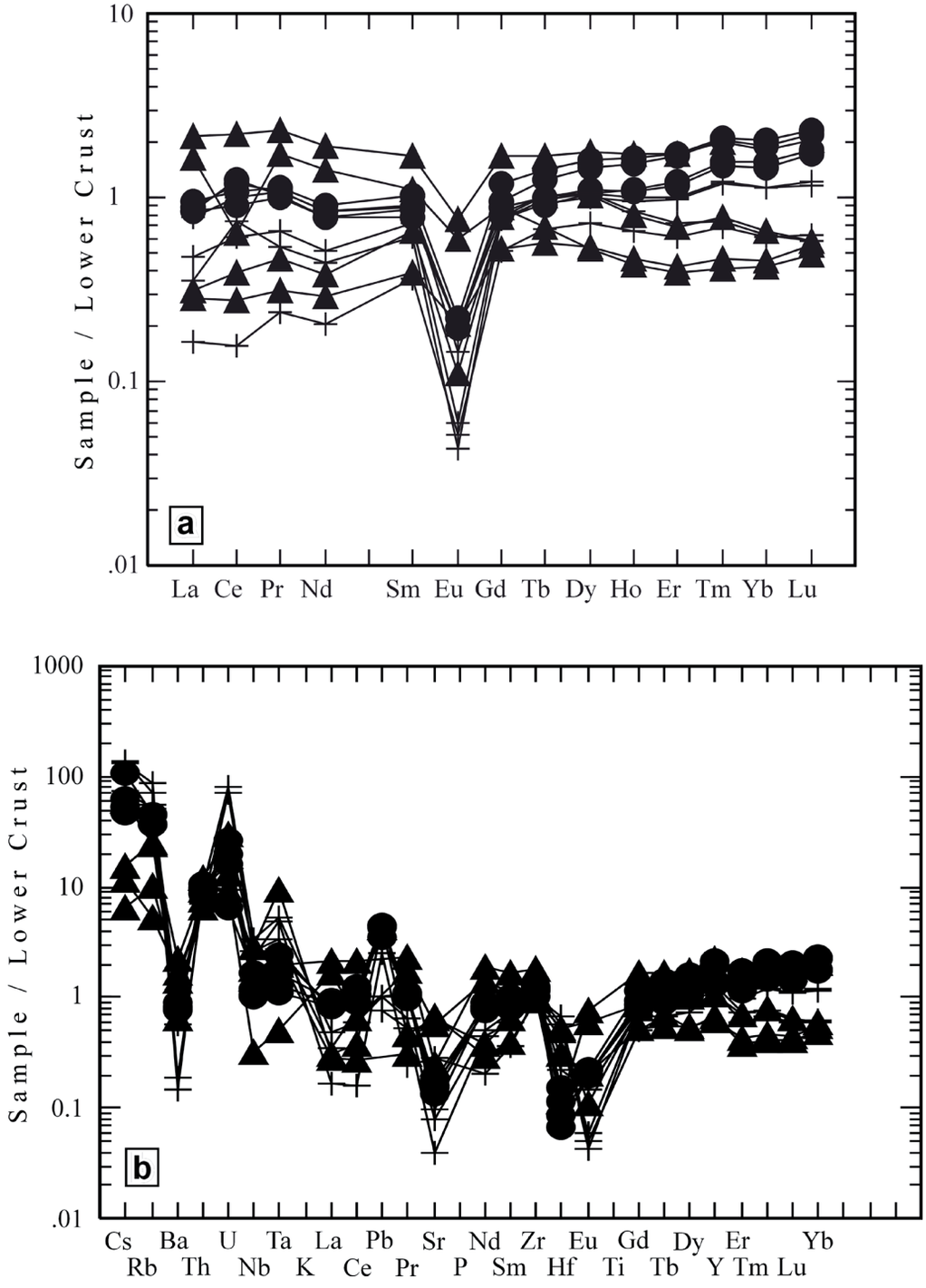

Figure 11a:
(a) Lower crust-normallized trace element profiles of orthogneisses, leucgranites and dyke rocks of the southern Menderes Massif. **(b)** A multi-element spider diagram normalized against lower crust [157]. Pluses, leucogranites; close circles, orthogneisses; close triangles, dykes.

S–SSW deformation along the southern Menderes shear zone resulted in shearing of leucogranites into parallelism with the shear-zone foliation and generation of S-C fabrics.

The extension might have also resulted in adiabatic decompressional melting during the latest stages of extensional deformation. This would explain almost entirely undeformed and/relatively less deformed mica-tourmaline leucogranitic dykes in the southern Menderes Massif. Diachronous thrusting and normal faulting during the latest stages of the main Menderes metamorphism, but before the final motion along the top-to-the-N–NNE southern Menderes shear zone; tectonic burial by imbrication and crustal thickening at depth may also have been assisted by normal faulting at higher structural levels.

6.2. Orthogneisses

The presence of Precambrian orthogneisses and metagabbros with HP relicts structurally below the metasediments may indicate that the Menderes Massif consisted of three layers before the onset of the main Menderes metamorphism, comprising

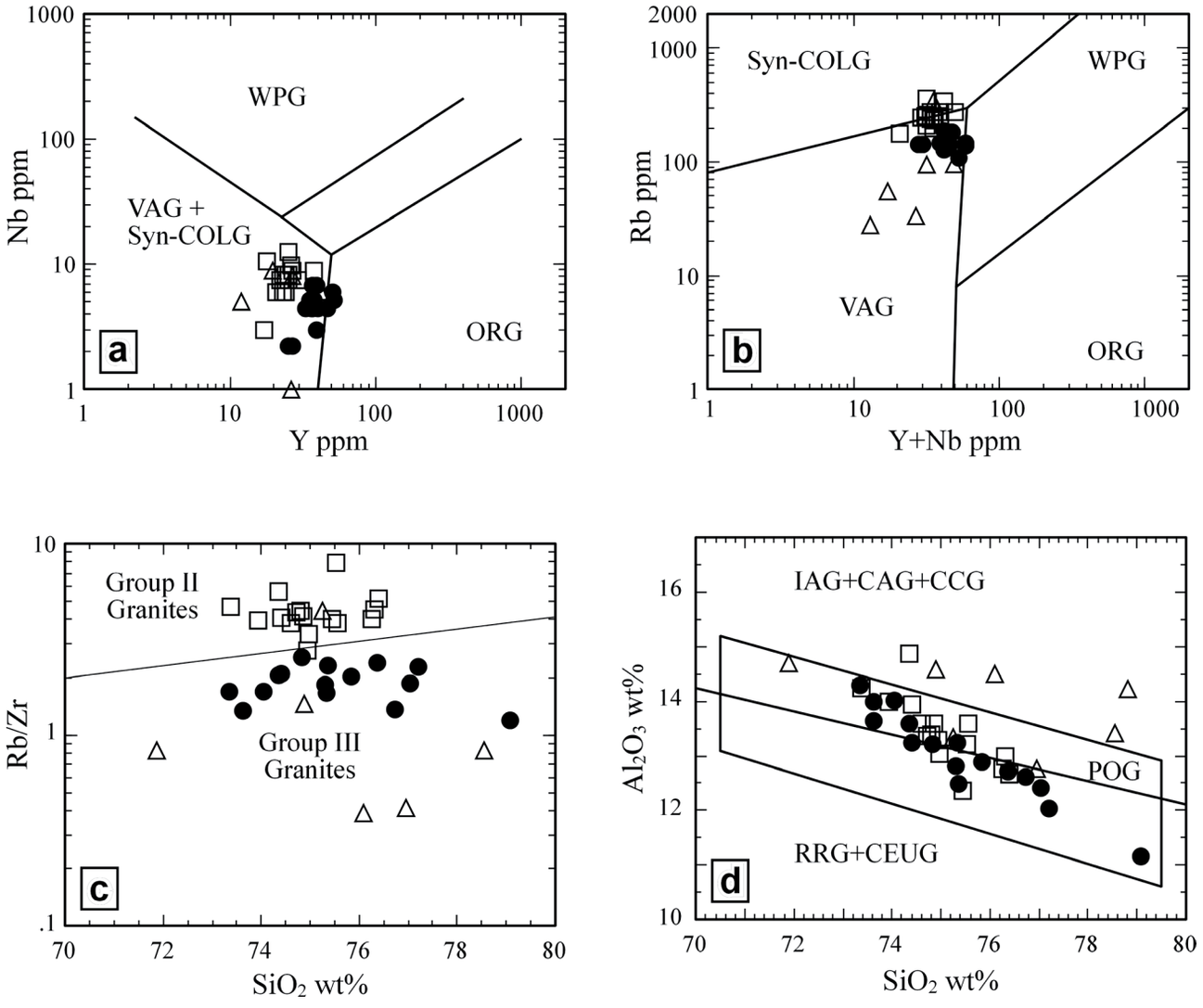

Figure 12: Tectonic discrimination diagrams. **(a)** Y vs Nb; **(b)** Y+Nb vs Rb [117]; **(c)** SiO_2 vs Rb/Zr [118] and **(d)** SiO_2 vs Al_2O_3 [119]. Open squares, leucogranites; close circles, orthogneisses; open triangles, dykes.

from top to bottom, Palaeozoic to Cenozoic metasediments, Precambrian orthogneisses, and metasediments exposed in the central Menderes Massif. They show evidence for inverted metamorphism. The upper schist layer behaved ductilely, as expressed by the development of regional top-to-the-N–NNE foliation and foliation-parallel F_2 folds. The granitoid middle layer became relatively weak during crustal thickening, leading to distinct rheologic behaviour in which remobilized granites acquired a gneissic texture at deep crustal levels, and were then thrust northward onto the metasediments of the central Menderes Massif. The well-documented orthogneiss klippen above schists along the northern margin of Büyük Menderes Graben [e.g., 40, 146, 147] and along the southern margin of the Gediz Graben [38] support this contention; they were later exhumed in the footwall of top-to-the-S–SSW extensional southern Menderes shear zone.

6.3. Tectono-Stratigraphic Implications of Tourmalines

Chemistry suggests that tourmaline in the tourmaline-rich pebble from the Gökçay metaconglomerate formed in a sedimentary environment, as did those in massive to laminated tourmalinites in a number of schists from the metasediments comprising the so-called '*cover*' of the Menderes Massif [83–85]. By contrast massive tourmaline-rich rocks (such as the quartz-tourmaline lenses near Labranda) within leucogranite consist of tourmaline of clearly granitic pedigree, and are similar to magmatic tourmalines disseminated in the leucogranite and making up granite-hosted quartz-tourmaline nodules.

If this use of tourmaline as a petrogenetic indicator is valid, the tourmaline-rich pebble from the Gökçay metaconglomerate is of sedimentary derivation and was probably sourced from the metasedimentary '*cover*' units. If so, the Gökçay metaconglomerate may be an intraformational rather than basal conglomerate as previously interpreted by Konak *et al.* [105] and Dora *et al.* [106]. Furthermore, if it is indeed intraformational, a crucial piece of evidence that has been

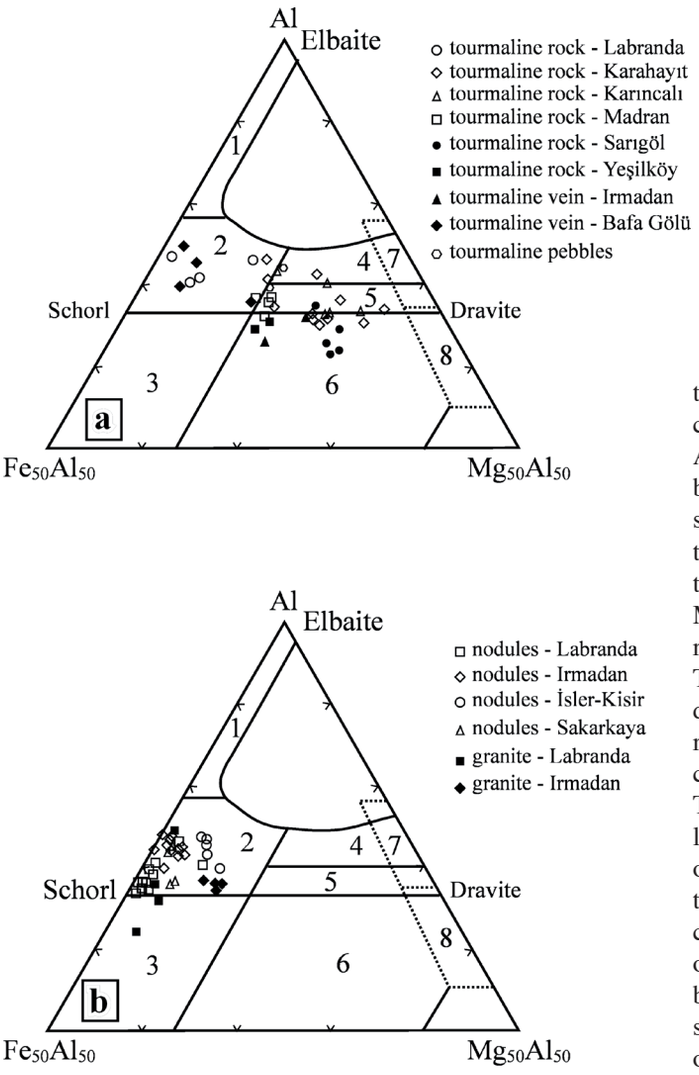

Figure 13: Compositions of Menderes Massif tourmalines plotted in terms of Al-Fe(tot)-Mg.
(a) mainly sediment-related tourmalines,
(b) granite-related tourmalines. Fields from Henry and Guidotti [111]. 1– Li-rich granitoid pegmatites and aplites, 2– Li-poor granitoids and their associated pegmatites and aplites, 3– Fe^{3+}-rich quartz-tourmaline rocks (hydrothermally altered granites), 4– metapelites and metapsammites coexisting with an Al-saturating phase, 5– metapelites and metapsammites not co-existing with an Al-saturating phase, 6– Fe^{3+}-rich quartz-tourmaline rocks, calc-silicate rocks, and metapelites, 7– low-Ca metaultramafics and Cr, V-rich metasediments, 8– metacarbonates and metapyroxenites.

used in support of a major (Pan-African) unconformity at the so-called "core (orthogneiss)-cover (schist)" boundary [106] is rendered invalid.

In this case, the tourmaline-bearing pebbles in the Gökçay conglomerate cannot be derived from a granitic source but must have been derived from an older metasedimentary sequence. The geochemistry of tourmalines is therefore consistent with field relations that the leucogranites are much younger than the metasediments containing metaconglomerates and that there is no reason for conglomerates to have tourmalines as in leucogranites. This piece of evidence also confirms that the boundary between so-called '*core-cover*' rocks is an Alpine extensional shear zone rather than an unconformity.

7. Conclusions

The tectonic evolution of the Menderes Massif involves two distinct periods: (i) crustal thickening and thermal maturation followed by (ii) syn- to post-convergence extension and thinning of previously thickened crust. The latest Palaeogene collision between the Sakarya continent to the north and the Anatolide-Tauride platform to the south across the northern branch of Neotethys was responsible for nappe stacking along south-verging thrust faults, crustal thickening and burial of the massif area. Burial resulted in widespread Barrovian-type amphibolite- to greenschist-facies metamorphism (main Menderes metamorphism) with temperatures and pressures ranging from 430 to 730 °C and from 5 to 11 kbar, respectively. The metamorphism was associated with top-to-the-N–NNE deformation, up-dip with respect to the present-day configuration of foliation, and was largely controlled by horizontal compression linked to the kinematics of nappe translation. The presence of layers of leucocratic granitic material – leucosome rimmed by melanosomes or *lit-part-lit* intrusion of granite – in the fertile pelitic-semipelitic schists close to the contact with the orthogneisses suggests that the thickened crust possibly experienced crustal anatexis during the climax of the main Menderes metamorphism. Partial melting probably resulted from shear heating along the top-to-the-N–NNE southern Menderes shear zone that emplaced schist onto the orthogneisses. Partial melting and distribution of leucogranitic melt weakened the crust and triggered the transition from crustal thickening to late orogenic collapse during which the southern Menderes shear zone was reactived as a top-to-the-S–SSW extensional shear zone. The crust thinned and the orthogneisses and the intrusive leucogranites were deformed and exhumed in the footwall of the southern Menderes shear zone. There, the southern Menderes shear zone marks a sudden jump in metamorphic gradient from upper amphibolite facies in the footwall to low amphibolite–greenschist facies in the hanging wall, suggesting a missing crustal section ~ 7-km thick [76]. The preserved HT-MP metamorphic assemblages in the schists of the southern Menderes Massif are, on the other hand, attributed to the early stage of burial of tectonic slices during the southward translation of Lycian Nappes above the Menderes Massif area [69, 70], whereas subsequent burial causing the main Menderes metamorphism is attributed to back-thrusting of Lycian and Menderes nappes [37].

Elsewhere in the Menderes Massif, extensional shear zones and now low-angle normal faults (detachments) were responsible for progressive uplift and exhumation of the high-grade metamorphic rocks in the footwall while Miocene continental sediments were deposited in extensional basins

formed above these detachments (e.g., the Gediz and Büyük Menderes detachment faults). The available data suggests that the extension of previously thickened crust in southwestern Turkey commenced by the latest Oligocene–Early Miocene time. The literature also argues that orogenic collapse cannot alone explain the late-orogenic extension and that a subduction roll-back process and back-arc extension must have contributed to the crustal extension to some extent. The southern Menderes Massif therefore records a complex history of crustal thickening, metamorphism, deformation, migmatization, partial melting, leucogranite emplacement and exhumation during which granitic melts played important roles. The structural history involves first N–NNE-directed displacements along south-facing thrust fault(s) (southern Menderes shear zone) and then S–SSW-directed extension in the footwall of the reactivated southern Menderes shear zone.

This study interprets the interplay between crustal thickening and extensional exhumation of the southern Menderes Massif, using evidence from field observations, structural analyses and geochemistry of leucogranites and tourmalines. It is interdisciplinary because determining the intimate link among crustal thickening, metamorphism, migmatization, magma generation and emplacement, and extension in exhumed metamorphic terranes requires an interdisciplinary approach involving field relations, structural analysis and analytical data (geochemistry, petrology, geochronology, thermochronology, *P–T* paths and possibly geophysics). Our model needs further testing using detailed geochronology, as demonstrated by the works of Keay *et al*. [32] concerning the Naxos dome (central Aegean) and of Whitney and Hamilton [148] and Whitney *et al*. [149] concerning the Niğde and Kırşehir massifs (central Anatolia). Finally, we would like to emphasize that future interdisciplinary research in this part of the world will lead to significant advances, not only in understanding the Menderes Massif and southwestern Turkey but also the close link among migmatization, crustal magmatism and extension.

Finally, this discussion confirms that leucogranites in collisional terranes are a key to understanding of interplay between crustal thickening and late-orogenic extension. The conclusions reached here can have more regional implications, for example that shear heating along thrust fault(s) during latest increments of contractional deformation during crustal thickening or decompressional melting in the footwall of normal fault(s) during crustal thinning does not explain alone the origin of migmatization, crustal magmatism (magma generation and emplacement) and deformation. Instead, these processes are effective at different stages of tectono-magmatic-metamorphic evolution of orogens and contribute to the transition from crustal thickening to thinning.

Acknowledgements

This research was partially funded by Middle East Technical University Research Foundation grants (AFP–2000-03-09-02, AFP–2001-03-09-04), TÜBİTAK grant YDABÇAG-221/A and by the Turkish Academy of Sciences in the framework of the Young Scientist Award Program (EA-TÜBA-GEBİP/2001-1-1) to EB. Thanks to W.D. Sinclair who kindly provided the photomicrograph of the tourmaline-rich pebble and arranged for the microprobe analyses reported herein to be done in the laboratories of the Geological Survey of Canada; J.A.R. Stirling performed the analyses, and G. Pringle calculated the structural formulae. We are grateful to Osman Candan for providing the metaconglomerate sample and to Cahit Helvacı for logistical help. The authors would also like to express sincere thanks to the reviewers whose careful comments and useful criticisms have greatly improved an earlier version of the manuscript.

References

[1] C. Davidson, L.S. Hollister, S.M. Schmid, Role of melt in the formation of a deep-crustal compressive shear zone: The MacLaren Glacier metamorphic belt, South Central Alaska, *Tectonics* 11 (1992) 348–359.

[2] C. Davidson, D.E. Grujic, L.S. Hollister, S.M. Schmid, Metamorphic reactions related to decompression and synkinematic intrusion of leucogranite, High Himalayan Crystallines, Bhutan, *J. Metamorph. Geol.* 15 (1997) 393–612.

[3] M.P. Searle, R.R. Parrish, K.V. Hodges, A. Hurford, M.W. Ayres, M.J. Whitehouse, Shisha Pangma leucogranite, South Tibetan Himalaya; field relations, geochemistry, age, origin, and emplacement, *J. Geol.* 105 (1997) 295–317.

[4] M.P. Searle, S.R. Noble, A.J. Hurford, D.C. Rex, Age of crustal melting, emplacement and exhumation history of the Shivling leuocgranite, Garhwal Himalaya, *Geo. Mag.* 136 (1999) 513–525.

[5] T.M. Harrison, M. Grove, O.M. Lovera, E.J. Catlos, A model for the origin of Himalayan anatexis and inverted metamorphism, *J. Geophys. Res.* 103 (1998) 27017– 27032.

[6] T.M. Harrison, M. Grove, K.D. McKeegan, C.D. Coath, O.M. Lovera, O. Le Fort, Origin and episodic emplacement of the Manaslu intrusive complex, Central Himalaya, *J. Petrology* 40 (1999) 3–19.

[7] P.I. Nabelek, M. Liu, Leucogranites in the Black Hills, South Dakota: the consequence of shear heating during continental collision, *Geology* 27 (1999) 523–536.

[8] P.I. Nabelek, M. Liu, Petrologic and thermal constraints on the origin of leucogranites in collisional orogens, *Trans. Royal Soc. Edinburgh: Earth Sci.* 95 (2004) 73–85.

[9] J.D. Walker, M.W. Martin, S.A. Bowring, M.P. Searle, D.J. Waters, K.V. Hodges, Metamorphism, melting, and extension: age constraints from the High Himalayan slab of southeast Zanskar and northwest Lahaul, *J. Geology* 107 (1999)473–495.

[10] P. Rey, O. Vanderhaeghe, C. Teyssier, Gravitational collapse of the continental crust: definition, regimes and modes, *Tectonophysics* 342 (2001) 435– 449.

[11] C.G. Daniel, L.S. Hollister, R.R. Parrish, D. Grujic, Exhumation of the Main Central Thrust from lower crustal depths, Eastern Bhutan Himalaya, *J. Metamorph. Geol*. 21 (2003) 317–334.

[12] M.P. Searle, L. Godin, The south Tibetan detachment and the Manslu leucogranite: a structural reinterpretation and restoration of the Ananpurna-Manuslu Himalaya, Nepal, *J. Geol*. 111 (2003) 505–523.

[13] J.A. Gilotti, W.C. McClelland, Leucogranites and the time of extension in the east Greenland Caledonides, *The Jour. Geol.* 113 (2005) 399–417.

[14] B.J. Johnson, Extensional shear zones, granitic melts, and linkage of overstepping normal faults bounding the Shuswap metamorphic core complex, British Columbia. *GSA Bull*. 118 (2006) 366–382.

[15] B.F. Miller, A.H. Fetter, K.G. Stewart, Plutonism in three orogenic pulses, Eastern Blue Ridge Province, southern Appalachians, *GSA Bulletin* 118 (2006) 171–184.

[16] B.C. Burchfiel, C. Zhiliang, K.V. Hodges, L. Yuping, L. Royden, D. Changrong, X. Jiene, *The South Tibetan Detachment System, Himalayan Orogen: Extension Contemporaneous with and Parallel to Shortening in a Collisional Mountain Belt*. Geol Soc America Spec Publ 269 (1992), 41 p.

[17] B.C. Burchfiel, L.H. Royden North-south extension within the convergent Himalayan region, *Geology* 13 (1985) 679–682.

[18] M.A. Murphy, T.M. Harrison, Relationship between leucogranites and the Qomolangma detachment in the Rongbuk valley, south Tibet, *Geology* 27 (1999) 831–834.

[19] M.P. Searle, R.L. Simpson, R.D. Law, R.R. Parrish, D.J. Waters, The structural geometry, metamorphic and magmatic evolution of the Everest massif, High Himalaya of Nepal-South Tibet, *J. Geol. Soc. London* 160 (2003) 345–366.

[20] B.V. Aguado, M.R. Azevedo, U. Schakteggeri, J.R.M. Catalán, J. Nolan, U–Pb zircon and monazite geochronology of Variscan magmatism related to syn-convergence extension in Central Northern Portugal, *Lithos* 82 (2005) 169–184.

[21] A. Aranguren, J.M. Tubia, J.L. Bouchez, J.L. Vigneresse, The Guitiriz granite, Variscan belt of northern Spain: Extension-controlled emplacement of magma during tectonic escape, *Earth Planet. Sci. Lett*. 139 (1996) 165–176.

[22] D.H.W. Hutton, T.J. Dempster, P.E. Brown, S.D. Becker, A new mechanism of granite emplacement: intrusion in active extensional shear zones, *Nature* 343 (1990) 452–455.

[23] D.A. Foster, C. Schafer, C.M. Fanning, D.W. Hyndman, Relationships between crustal partial melting, plutonism, orogeny, and exhumation: Idaho–Bitterroot batholith, *Tectonophysics* 342 (2001) 313–350.

[24] M. Liu, Cenozoic extension and magmatism in the North American Cordillera: the role of gravitational collapse, *Tectonophysics* 342 (2001) 407–433.

[25] O. Vanderhaeghe, Pervasive melt migration from migmatites to leucogranite in the Shuswap metamorphic core complex, Canada: control of regional deformation, *Tectonophysics* 312 (1999) 35–55.

[26] O. Vanderhaeghe, J.-P. Burg, C. Teyssier, Exhumation of migmatitic terrains in the hinterland of two collapsed orogens, in: U. Ring, M. Brandon, S. Willet, G. Lister, (Eds), *Exhumation Processes: Normal Faulting, Ductile Flow and Erosion*. Geological Society, London, Special Publications 154, (1999a) 181-184.

[27] O. Vanderhaeghe, C. Teyssier, R. Wysoczanski, Structural and geochronologic constraints on the role of partial melting during the formation of the Shuswap metamorphic core complex at the latitude of the Thor–Odin dome, British Columbia, *Can. J. Earth Sci*. 36 (1999b) 917– 943.

[28] O. Vanderhaeghe, C. Teyssier, Partial melting and flow of orogens, *Tectonophysics* 342 (2001) 451– 472.

[29] P. Ledru, G. Courrioux, C. Dallain, J.M. Lardeaux, J.M. Montel, O. Vanderhaeghe, G. Vitel, The Velay dome (French Massif Central): melt generation and granite emplacement during orogenic evolution, *Tectonophysics* 342 (2001) 207–237.

[30] P. Gautier, J.-P. Brun, J. Jolivet, Structure and kinematics of Upper Cenozoic extensional detachment on Naxos and Paros (Cyclades islands, Greece), *Tectonics* 12 (1993) 1180–1194.

[31] P. Gautier, J.-P. Brunn, Ductile crust exhumation and extensional detachments in the central Aegean (Cyclades and Evvia islands), *Geodinam. Acta* 7 (1994) 57–85.

[32] S. Keay, G. Lister, I. Buick, The timing of partial melting, Barrovian metamorphism and granite intrusion in the Naxos metamorphic core complex, Cyclades, Aegean Sea, Greece, *Tectonophysics* 342 (2001) 275–312.

[33] O. Vanderhaeghe, C. Teyssier, Crustal-scale rheological transitions during late-orogenic collapse, *Tectonophysics* 335 (2001b) 211–228.

[34] E. Bozkurt, R.G. Park, Southern Menderes Massif: an incipient metamorphic core complex in western Anatolia, Turkey, *J. Geol. Soc. London* 151 (1994) 213–216.

[35] E. Bozkurt, R.G. Park, Evolution of a mid-Tertiary extensional shear zone in the southern Menderes Massif, Western Turkey, *Soc. Géol. France Bull.* 168 (1997a) 3–14.

[36] E. Bozkurt, R.G. Park, Microstructures of deformed grains in the augen gneisses of southern Menderes Massif and their tectonic significance, *Geol. Rundschau* 86, (1997b) 103–119.

[37] E. Bozkurt, R.G. Park, The structure of the Palaeozoic schists in the southern Menderes Massif, western Turkey: a new approach to the origin of the main Menderes metamorphism and its relation to the Lycian nappes, *Geodinam. Acta* 12 (1999) 25–42.

[38] R. Hetzel, U. Ring, C. Akal, M. Troesch, Miocene NNE- directed extensional unroofing in the Menderes Massif, southwestern Turkey, *J. Geo. Soc. London* 152 (1995) 639–654.

[39] R. Hetzel, R.L. Romer, O. Candan, C.W. Passchier, Geology of the Bozdağ area, central Menderes Massif, SW Turkey: Pan-African basement and Alpine deformation, *Geo. Rundschau* 87 (1998) 394–406.

[40] E. Bozkurt, Late Alpine evolution of the central Menderes Massif, western Anatolia, Turkey, *Inter. J. Earth Sci*. 89 (2001b) 728–744.

[41] E. Bozkurt, Granitoid rocks of the southern Menderes Massif (southwest Turkey): field evidence for Tertiary magmatism in an extensional shear zone, *Inter. J. Earth Sci*. 93 (2004) 52–71.

[42] E. Bozkurt, Extensional vs contractional origin for the southern Menderes shear zone, southwest Turkey: tectonic and metamorphic implications. *Geo. Mag*. (2006) [in press].

[43] E. Bozkurt, M. Satır, New Rb-Sr geochronology from the southern Menderes Massif (southwestern Turkey) and its tectonic significance, *Geol. Jour*. 35 (2000) 285–296.

[44] E. Bozkurt, R. Oberhänsli, Menderes Massif (western Turkey): structural, metamorphic and magmatic evolution – a synthesis, *Inter. J. Earth Sci.* 89 (2001) 679–708.

[45] K. Gessner, S. Piazolo, T. Güngör, U. Ring, A. Kröner, C.W. Passchier, Tectonic significance of deformation patterns in granitoid rocks of the Menderes nappes, Anatolide belt, southwest Turkey, *Inter. J. Earth Sci.* 89 (2001) 766–780.

[46] E. Gökten, Ş. Havzaoğulu, Ö. Şan, Tertiary evolution of the central Menderes Massif based on structural investigations of metamorphics and sedimentary cover rocks between Salihli and Kiraz (western Turkey), *Inter J Earth Sci* 89 (2001) 745–756.

[47] V. Işık, O. Tekeli, Late orogenic crustal extension in the northern Menderes Massif (western Turkey): evidence for metamorphic core complex formation, *Inter. J. Earth Sci.* 89 (2001) 757–765.

[48] A.L.W. Lips, D. Cassard, H. Sözbilir, H. Yılmaz, Multistage exhumation of the Menderes Massif, western Anatolia (Turkey), *Inter. J. Earth Sci.* 89 (2001) 781–792.

[49] V. Işık, G. Seyitoğlu, İ. Çemen, Ductile-brittle transition along the Alaşehir detachment fault and its structural relationship with the Simav detachment fault, Menderes Massif, western Turkey, *Tectonophysics* 374 (2003) 1–18.

[50] G. Seyitoğlu, V. Işık, İ. Çemen, Complete Tertiary exhumation history of the Menderes Massif, western Turkey: an alternative working hypothesis, *Terra Nova* 16 (2004) 358–363.

[51] E.J. Catlos, İ. Çemen, Monazite ages and the evolution of the Menderes Massif, western Turkey, *Inter. J. Earth Sci.* 94 (2005) 204–217.

[52] U. Ring, A.S. Collins, U-Pb SIMS dating of syn-kinematic granites: Timing of core-complex formation in the northern Anatolide belt of western Turkey, J. Geol. Soc. London 162 (2005) 289–298.

[53] A. Koçyiğit, H. Yusufoğlu, E. Bozkurt, Evidence from the Gediz Graben for episodic two-stage extension in western Turkey, *J. Geol. Soc. London* 156 (1999) 605–616.

[54] E. Bozkurt, Timing of Extension on the Büyük Menderes Graben, Western Turkey and its tectonic implications, in: E. Bozkurt, J.A. Winchester, J.D.A. Piper, (Eds), *Tectonics and Magmatism in Turkey and the Surrounding Area*. Geological Society, London, Special Publications 173, 2000, pp. 385–403.

[55] E. Bozkurt, Neotectonics of Turkey – a synthesis, *Geodinam. Acta* 14 (2001a) 3–30.

[56] G. Seyitoğlu, O. Tekeli, İ. Çemen, Ş. Şen, V. Işık, The role of the flexural rotation/rolling hinge model in the tectonic evolution of the Alaşehir Graben, western Turkey, *Geo. Mag.* 139 (2002) 15–26.

[57] E. Bozkurt, H. Sözbilir, Tectonic evolution of the Gediz Graben: field evidence for an episodic, two-stage extension in western Turkey, *Geo. Mag.* 141 (2004) 63–79.

[58] O. Kaya, E. Ünay, G. Saraç, S. Eichhorn, S. Hassenrück, A. Knappe, A. Pekdeğer, S. Mayda, Halitpaşa transpressive zone: implications for an Early Pliocene compressional phase in central western Anatolia, Turkey, *Turkish J. Earth Sci.* 13 (2004) 1–13.

[59] E. Bozkurt, S.K. Mittwede, Introduction: Evolution of Neogene extensional tectonics of western Turkey, *Geodinam. Acta* 18 (2005) 153–165.

[60] E. Bozkurt, B. Rojay, Episodic, two-stage Neogene extension and short-term intervening compression in western Anatolia: field evidence from the Kiraz basin and Bozdağ horst, *Geodinam. Acta* 18 (2005) 299–316.

[61] F. Erkül, C. Helvacı, H. Sözbilir, Evidence for two episodes of volcanism in the Bigadiç borate basin and tectonic implications for western Turkey, *Geol. Jour.* 40 (2005a) 545–570.

[62] F. Erkül, C. Helvacı, H. Sözbilir, Stratigraphy and geochronology of the Early Miocene volcanics in the Bigadiç borate basin, western Turkey, *Turkish J. Earth Sci.* 14 (2005b) 227–253.

[63] A. Koçyiğit, The Denizli graben-horst system and the eastern limit of western Anatolian continental extension: basin fill, structure, deformational mode, throw amount and episodic evolutionary history, SW Turkey, *Geodinam. Acta* 18 (2005) 167–28.

[64] B. Rojay, V. Toprak, C. Demirci, L. Süzen, Plio-Quaternary evolution of the Küçük Menderes Graben southwestern Anatolia, Turkey, *Geodinam. Acta* 18 (2005) 317–331.

[65] M. Tokçaer, S. Agostini, M.Y. Savaşçın, Geotectonic setting and origin of the youngest Kula volcanics (western Anatolia), with a new emplacement model, *Turkish J. Earth Sci.* 14 (2005) 143–166.

[66] Y. Yücel-Öztürk, C. Helvacı, M. Satır, Genetic relations between skarn mineralization and petrogenesis of the Evciler Granitoid, Kazdağ, Çanakkale, Turkey and comparison with world skarn granitoids, *Turkish J. Earth Sci.* 14 (2005) 225–280.

[67] E. Aldanmaz, Mineral chemical constraints on the Miocene calc-alkaline and shoshonitic volcanic rocks of western Turkey: disequilibrium phenocryst assemblages as indicators of magma storage and mixing conditions, *Turkish J. Earth Sci.* 15 (2006) 47–73.

[68] S. Özer, H. Sözbilir, İ. Özkar, V. Toker, B. Sarı, Stratigraphy of Upper Cretaceous-Palaeocene sequences in the southern and eastern Menderes Massif, *Inter. J. Earth Sci.* 89 (2001) 852–866.

[69] G. Rimmelé, R. Oberhänsli, B. Goffé, L. Jolivet, O. Candan, M. Çetinkaplan, First evidence of high-pressure metamorphism in the '*cover series*' of the southern Menderes Massif: tectonic and metamorphic implications for the evolution of the SW Turkey, *Lithos* 71 (2003a) 19–46.

[70] G. Rimmelé, L. Jolivet, R. Oberhänsli, B. Goffé, Deformation history of the high-pressure Lycian nappes and implications for tectonic evolution of SW Turkey, *Tectonics* 22 (2003b) 1007–1029.

[71] M.M. Evirgen, Menderes masifi kuzey kesiminde (Ödemiş-Bayındır-Turgutlu) gelişen metamorfizma ve bazı ender parajenezler [Metamorphism in the northern sector of the Menderes Massif (Ödemiş-Bayındır-Turgutlu) and some of the rare paragenesis], *Geol. Soc. Turkey Bull.* 22 (1979) 109–116.

[72] M.M. Evirgen, G. Ataman, Menderes Masifinin merkezi bölgesinin metamorfizmasının incelenmesi. izograd, basınç ve sıcaklık [Study of the metamorphism in the central Menderes Massif: Isograde, pressure and temperature], *Yerbilimleri* 7 (1981) 15–26. [in Turkish whith English abstract].

[73] M.M. Evirgen, G. Ataman, Etude du mètamorphisme de la zone centrale du Massif de Menderes. Isogrades, pressions et temperature, *Soc. Géol. France Bull.* 24 (1982) 309–319.

[74] J.R. Ashworth, M.M. Evirgen, Garnet and associated minerals in the southern margin of the Menderes Massif, southwestern Turkey, *Geo. Mag.* 121 (1984) 323–337.

[75] D.L. Whitney, E. Bozkurt, Metamorphic history of the southern Menderes Massif, western Turkey, *GSA Bull.* 114 (2002) 829–838.

[76] J.L. Régnier, U. Ring, C.W. Passchier, K. Gessner, T. Güngör, Contrasting metamorphic evolution of metasedimentary rocks from the Çine and Selimiye nappes in the Anatolide belt, western Turkey, *J. Metamorph. Geol.* 21 (2003) 699–721.

[77] E. Bozkurt, R.G. Park, J.A. Winchester, Evidence against the core/cover concept in the southern sector of the Menderes Massif. *Turkish Geology Workshop (Work in Progress on the Geology of Türkiye), 9–10 April, Keele*, (1992) p. 22.

[78] E. Bozkurt, R.G. Park & J.A. Winchester, Evidence against the core/cover interpretation of the southern sector of the Menderes Massif, west Turkey. *Terra Nova* 5 (1993) 445–451.

[79] E. Bozkurt, J.A. Winchester, R.G. Park, Geochemistry and tectonic significance of augen gneisses from the southern Menderes Massif (West Turkey), *Geo. Mag.* 132 (1995) 287–301.

[80] B. Erdoğan, Problem of core-mantle boundary of Menderes Massif, in: M. Anıl, A. Nazik (Eds), *Proceedings of the International Symposium on Eastern Mediterranean Geology, Adana*. Geosound 20, 1992, 314–315.

[81] B. Erdoğan, Menderes Masifinin kuzey kanadının stratigrafisi ve çekirdek-örtü ilişkisi [Stratigraphy of the northern margin of the Menderes massif and the core-mantle relations], *Abstracts of the Geological Congress of Turkey, Ankara, Turkey*, 1993, p 56.

[82] E. Bozkurt, R.G. Park, Discussion on the evolution of the southern Menderes Massif in SW Turkey as revealed by zircon dating, *J. Geol. Soc. London* 158 (2001) 393–395.

[83] S.K. Mittwede, İ.H. Karamanderesi, C. Helvacı, *Tourmaline-rich Rocks of the Southern Part of the Menderes Massif, Southwestern Turkey*, International Earth Sciences Colloquium on the Aegean Region 1995 Excursion Guide. Dokuz Eylül University, Department of Geological Engineering, İzmir, 1995a, 25 p.

[84] S.K. Mittwede, W.D. Sinclair, İ.H. Karamanderesi, C. Helvacı, Geochemistry of quartz-tourmaline nodules from Irmadan (Muğla-Yatağan), Türkiye, *Abstracts of the Second International Turkish Geology Worshop, September 6–8, 1995, Sivas, Turkey*, 1995b, p. 74.

[85] S.K. Mittwede, W.D. Sinclair, C. Helvacı, İ.H. Karamanderesi, Quartz-torumaline nodules in leucocratic metagranite, southern flank of the Menderes Massif, SW Turkey, *Tourmaline '97, International Symposium on Tourmaline Abstract Volume*, Czech Republic, 1997, pp. 57–58.

[86] E. Erdoğan, T. Güngör, The problem of the core–cover boundary of the Menderes Massif and an emplacement mechanism for regionally extensive gneissic granites, western Anatolia (Turkey), *Turkish J. Earth Sci.* 13 (2004) 15–36.

[87] E. Bozkurt, Deformation during main Menderes metamorphism (MMM) and its tectonic significance: evidence from Southern Menderes Massif, western Turkey. EUG VIII, Strasbourg, 9–13 April, *Terra Abstracts* 7 (1995) 176.

[88] E. Bozkurt, Metamorphism of Palaeozoic schists in the southern Menderes Massif: field, petrographic, textural and microstructural evidence, *Turkish J. Earth Sci.* 5 (1996) 105–121.

[89] R. Hetzel, T. Reischmann, Intrusion age of Pan-African augen gneisses in the southern Menderes Massif and the age of cooling after Alpine ductile extensional deformation, *Geo. Mag.* 133 (1996) 565–572.

[90] C. Dannat, *Geochemie, Geochronologie und ND-Sr-Isotopie der granitoiden Kerngneise des Menderes Massivs, SW Türkie*. PhD Thesis, Johannes Guternberg Universitat, Mainz, (1997) 120 p.

[91] S. Loos, T. Reischmann, The evolution of the southern Menderes Massif in SW Turkey as revealed by zircon datings, *J. Geol. Soc. London* 156 (1999) 1021–1030.

[92] K. Gessner, U. Ring, C.W. Passchier, T. Güngör, How to resist subduction: evidence for large-scale out-of-sequence thrusting during Eocene collision in western Turkey. J. Geol. Soc. London 158 (2001c) 769–784.

[93] A.M.C. Şengör, M. Satır, R. Akkök, Timing of tectonic events in the Menderes Massif, western Turkey: implications for tectonic evolution and evidence for Pan-African basement in Turkey, *Tectonics* 3 (1984) 693–707.

[94] M. Satır, H. Friedrichsen, The origin and evolution of the Menderes Massif, W-Turkey: A rubidium/strontium and oxygen isotope study, *Geol. Rundshau* 75 (1986) 703–714.

[95] U. Ring, K. Gessner, T. Güngör, C.W. Passchier, The Menderes Massif of western Turkey and the Cycladic Massif in the Aegean – do they really correlate? *J. Geol. Soc. London* 156 (1999) 3–6.

[96] O.E. Koralay, O.Ö. Dora, F. Chen, M. Satır, O. Candan, Geochemistry and geochronology of orthogneisses in the Derbent (Alaşehir) area, eastern part of the Ödemiş–Kiraz submassif, Menderes Massif: Pan-African magmatic activity, *Turkish J. Earth Sci.* 13 (2004) 37–61.

[97] K. Gessner, A.S. Collins, U. Ring, T. Güngör, Structural and thermal history of poly-orogenic basement: U–Pb gecohronology of granitoid rocks in the southern Menderes Massif, western Turkey, *J. Geol. Soc. London* 161 (2004) 93–101.

[98] R.D. Schuiling On the petrology, age and structure of the Menderes migmatite complex (SW Turkey), *MTA Bull.* 58 (1962) 71–84.

[99] E. Başarır, *Bafa Gölü Doğusunda Kalan Menderes Masifi Güney Kanadının Jeolojisi ve Petrografisi [Geology and Petrography of the Southern Sector of Menderes Massif in the East of Lake Bafa]*. Faculty of Science Publication, Ege University, 102 (1970) [in Turkish with English abstract].

[100] E. Başarır, *Çine Güneyindeki Metamorfitlerin Petrografisi ve Bireysel İndeks Minerallerin Doku İçerisindeki Gelişimleri [The Petrography of the Metamorphics Exposing to the South of Çine and the Growth of Individual Index Minerals Within the Metamorphic Texture]*, D.Sc. Thesis, İzmir, 79 p (1975).

[101] M.A. Çağlayan, E.M. Öztürk, Z. Öztürk, H. Sav, U. Akat, Menderes Masifi güneyine ait bulgular ve yapısal yorum [New findings in the southern sector of the Menderes Massif and their structural interpretation], *Jeoloji Mühendisliği* 10 (1980) 9–19 [in Turkish with English abstract].

[102] A. Öztürk, A. Koçyiğit, Selimiye-Beşparmak yöresindeki (Muğla) Menderes Masifi kayalarının stratigrafisi [Stratigraphy of the rocks of the Menderes Massif in the Selimiye-Beşparmak (Muğla) region], *Geol. Soc. Turkey Bull.* 25 (1982) 67–72. [in Turkish whith English abstract].

[103] A. Öztürk, A. Koçyiğit, Menderes grubu kayalarının temel-örtü ilişkisine yapısal bir yaklaşım (Selimiye-Muğla) [A structural approach to the basement-cover relationship in the Menderes Group rocks (Selimiye-Mugla)], *Geol. Soc. Turkey Bull.* 26 (1983) 99–106. [in Turkish whith English abstract].

[104] N. Konak, A discussion on the core-cover relationships on the basis of recent observations (Menderes Massif), *Abstract of Geological Congress of Turkey, Ankara*, 1985, p 33.

[105] N. Konak, N. Akdeniz, E.M. Öztürk, Geology of the south of Menderes Massif, in: *Guide Book for the Field Excursion Along Western Anatolia, Turkey, IGCP Project No. 5, Correlation of*

Variscan and Pre-Variscan Events of the Alpine-Mediterranean Mountain Belt, Field Meeting, Turkey. General Directorate of Mineral Research and Exploration. Ankara, 1987, pp. 42–53.

[106] O.Ö. Dora, O. Candan, S. Dürr, R. Oberhänsli, New evidence on the geotectonic evolution of the Menderes Massif, in: Ö. Pişkin, M. Ergün, M.Y. Savaşçın, G. Tarcan (Eds), *Proceedings of International Earth Science Colloqium on Aegean Region 1995, İzmir*, Volume I, 1997, pp. 53–72.

[107] V. Işık, O. Tekeli, G. Seyitoğlu, The Ar^{40}/Ar^{39} age of extensional ductile deformation and granitoid intrusion in the northern Menderes core complex: implications for the initiation of extensional tectonics in western Turkey, *J. Asian Earth Sci*. 23 (2004) 555–566.

[108] L. Jolivet, G. Rimmelé, R. Oberhänsli, B. Goffé, O. Candan, Correlation of syn-orogenic tectonic and metamorphic events in the Cyclades, the Lycian nappes and the Menderes Massif: Geodynamic implications, *Soc. Géol. France Bull*. 175 (2004) 217–238.

[109] U. Ring, C. Johnson, R. Hetzel, K. Gessner, Tectonic denudation of a Late Cretaceous–Tertiary collisional belt: regionally symmetric cooling patterns and their relation to extensional faults in the Anatolide belt of western Turkey, *Geo. Mag*. 140 (2003) 421–441.

[110] U. Ring, A. Willner, W. Lackmann, Stacking of nappes with different Pressure–temperature paths: an example from the Menderes nappes of western Turkey, *Am. J. Sci*. 301 (2001) 912–944.

[111] D.J. Henry, C.V. Guidotti, Tourmaline as a petrogenetic indicator mineral: an example from staurolite-grade metapelites of NW Maine, *Am. Min*. 70 (1985) 1–15.

[112] P.A. Floyd, P.R. Castillo, Geochemistry and petrogenesis of Jurassic ocean crust basalts, ODP Leg 129, Site 801, in: R. Larson, Y. Launcelot *et al*. (Eds), *Proccedings of ODP, Scientific Results* 129, 1992, 361–388.

[113] J.A. Winchester, C.R. Van Staal, J.P. Langton, The Ordovician volcanics of the Elmtree-belledune inlier and their relationships to volcanics of the northern Miramichi Highlands, New Brunswick, *Can. J. Earth Sci*. 29 (1992) 1430–1447.

[114] C.J. Ottley, D.G. Pearson, G.J. Irvine, A routine method for the dissolution of geological samples for the analysis of REE and trace elements via ICP-MS, in: J.G. Holland, S.D. Tanner, (Eds), *Plasma Source Mass Spectrometry: Applications and Emerging Technologies*. The Royal Society of Chemistry, Cambridge, 2003, 221–230.

[115] K.G. Cox, J.D. Bell, R.J. Pankhurst *The Interpretation of Igneous Rocks*, London, Allen and Unwin, (1979) 450 p.

[116] J.A. Winchester, P.A. Floyd Geochemical discrimination of different magma series and their differentiation products using immobile elements, *Chem. Geol*. 20 (1977) 325–343.

[117] J.A. Pearce, N.B.W. Harris, A.G.W. Tindle, Trace element discrimination diagrams for the tectonic interpretation of granitic rocks, *J. Petrology* 25 (1984) 956–983.

[118] N.B.W. Harris, J.A. Pearce, A.G. Tindle, Geochemical characteristics of collision-zone magmatism, in: M.P. Coward, A.C. Ries (Eds), *Collision Tectonics*, Geological Society, London, Special Publications 19, 1986, pp. 67–81.

[119] P.D. Maniar, P.M. Piccoli, Tectonic discrimination of granitoids, *GSA Bull*. 101 (1989) 635–643.

[120] A. Kassoli-Fournaraki, Chemical variations in tourmalines from pegmatite occurrences in Chalkidiki Peninsula, northern Greece, *Schweiz. Mineral. Petrogr. Mitt*. 70 (1990) 55–655.

[121] R.H. Hellingwerf, K. Gatedal, V. Gallagher, J.H. Baker, Tourmaline in the central Swedish ore district, *Mineral. Deposita* 29 (1994) 189–205.

[122] K. Michailidis, S. Sklavounos, I. Plimer, Chromian dravite from the chromite ores of the Vavdos area, Chalkidiki peninsula, northern Greece, *N. Jb. Mineral. Mh*. 11 (1995) 513–528.

[123] A. Rozendaal, L. Bruwer, Tourmaline nodules: indicators of hydrothermal alteration and Sn-Zn-(W) mineralization in the Cape Granite Suite, South Africa, *J. African Earth Sci*. 21 (1995) 141–155.

[124] S.-Y. Jiang, M.R. Palmer, Y.-H. Li, C.-J. Xue, Chemical compositions of tourmaline in the Yindongzi-Tongmugou Pb-Zn deposits, Qinling, China: implications for hydrothermal ore-forming processes, *Mineral. Deposita* 30 (1995) 225–234.

[125] M. Jingwen, Tourmalinite from northern Guangxi, China, *Mineral. Deposita* 30 (1995) 235–245.

[126] K. Michailidis, A. Kassoli-Fournaraki, Tourmaline concentrations in migmatitic metasedimentary rocks of the Riziana and Kolchiko areas in Macedonia, northern Greece, *Eur. J. Mineral*. 6 (1994) 557–569.

[127] I. Garba, Tourmalinization related to Late Proterozoic–Early Palaeozoic lode gold mineralization in the Bin Yauri area, Nigeria, *Mineral. Deposita* 31 (1996) 201–209.

[128] J.M. Cleland, G.B. Morey, P.L. McSwiggen, Significance of tourmaline-rich rocks in the North Range Group of the Cuyana iron range, east-central Minnesota, *Econ. Geol*. 91 (1996) 1282–1291

[129] S.K. Mittwede, C. Helvacı, İ.H. Karamanderesi, N. Kun, O. Candan, Modes and implications of tourmaline occurrences in the Menderes Massif, western Anatolia, Türkiye, in: M. Anıl, A. Nazik (Eds), *Proceedings of the International Symposium on Eastern Mediterranean Geology, Adana*. Geosound 20, (1992) 179–190.

[130] J.F. Slack, N. Herriman, R.G. Barnes, I.R. Plimer, Stratiform tourmalinites in metamorphic terranes and their geologic significance, *Geology* 12 (1984) 713–716.

[131] J.L. Pouchou, F. Pichoir, A new model for quantitative X-ray microanalysis, part I: application to the analysis of homogeneous samples, *Recherche Aerospatiale* 1984-3, (1984) 13–38

[132] M. Wilke, P.I. Nabelek, M.D., B and Li in metapelites from the Proterozoic Terrane in the Black Hills, South Dakota, USA: implications for the origin of leucogranitic magmas, *Am. Mineralogist* 87 (2002) 491–500.

[133] M. Brown, G.S. Solar, Shear-zone systems and melts: feedback relations and self-organization in orogenic belts, *J. Struct. Geol*. 20 (1998b) 211– 227.

[134] Y. Zhu, Y. Shi, Shear heating and partial melting of granite: thermal structure of overthrusted terrains in the Greater Himalaya, Chinese J. Geophys. 33 (1990) 341–351.

[135] P.C. England, P. Molnar, The interpretation of inverted metamorphic isograds using simple physical calculations, *Tectonics* 12 (1993) 145– 157.

[136] P.J. Treloar, Thermal controls on early-Tertiary, short-lived, rapid regional metamorphism in the NW Himalaya, Pakistan, *Tectonophysics* 273 (1997) 77–104.

[137] P.I. Nabelek, M. Liu, M.-L. Sirbescu, Thermo-rheological, shear

heating model for leucogranite generation, metamorphism, and deformation during the Proterozoic Trans-Hudson orogeny, Black Hills, South Dakota, *Tectonophysics* 342 (2001) 371– 388.

[138] T.M. Harrison, O.M. Lovera, M. Grove, New insights into the origin of two contrasting Himalayan belts, *Geology* 25 (1997) 899– 902.

[139] G.S. Solar, R.A. Pressley, M. Brown, R.D. Tucker, Granite ascent in convergent orogenic belts: testing a model, *Geology* 26 (1998) 711– 714.

[140] D.A. Schneider, M.A. Edwards, W.S.F. Kidd, K.M. Asif, L. Seeber, P.K. Zeitler, Tectonics of Nanga Parbat, western Himalaya; synkinematic plutonism within the doubly vergent shear zones of a crustal-scale pop-up structure, *Geology* 27 (1999) 999–1002.

[141] G.S. Solar, M. Brown, Petrogenesis of migmatites in Maine, USA: possible source of peraluminous leucogranite in plutons? *J. Petrology* 42 (2001) 789–823.

[142] J.-P. Burg, M. Brunel, D. Gapais, G.M. Chen, G.H. Liu, Deformation of leucogranites of the crystalline main central thrust sheet in southern Tibet (China), *J. Struct. Geol.* 6 (1984) 535– 542.

[143] D. Gapais, Shear structures within deformed granites: Mechanical and thermal indicators, *Geology* 17 (1989) 1144–1147.

[144] A. Tommasi, A. Vauchez, L.A.D. Fernandes, C.C. Porcher, Magma-assisted strain localization in an orogen-parallel transcurrent shear zone of southern Brazil, *Tectonics* 13 (1994) 421–437.

[145] M. Brown, G.S. Solar, Granite ascent and emplacement during contractional deformation in convergent orogens, *J. Struct. Geol.* 20 (1998a) 1365–1393.

[146] A.İ. Okay, Stratigraphic and metamorphic inversions in the central Menderes Massif: a new structural model, *Inter. J. Earth Sci.* 89 (2001) 709–727.

[147] S. Özer, H. Sözbilir, Presence and tectonic significance of Cretaceous rudist species in the so-called Permo-Carboniferous Göktepe Formation, central Menderes Massif, western Turkey, *Inter. J. Earth Sci.* 92 (2003) 397–404.

[148] D.L. Whitney, M.A. Hamilton, Timing of high-grade metamorphism in central Turkey and the assembly of Anatolia, *J. Geol. Soc. London* 161 (2004) 823–828.

[149] D.L. Whitney, C. Teyssier, A.K. Fayon, M.A. Hamilton, M. Heizler, Tectonic controls on metamorphism, partial melting, and intrusion: timing and duration of regional metamorphism and magmatism in the Nigde Massif, Turkey, *Tectonophysics* 376 (2002) 37–60.

[150] A.İ. Okay, O. Tüysüz, Tethyan sutures of northern Turkey, in: B. Durand, L. Jolivet, F. Horváth, M. Séranne (Eds), *The Mediterranean Basins: Tertiary Extension within the Alpine Orogen*. Geological Society, London, Special Publications 156, 1999, pp. 475–515.

[151] A.İ. Okay, Was the Late Triassic orogeny in Turkey caused by the collision of an oceanic plateau? in: E. Bozkurt, J.A. Winchester, J.D.A. Piper, (Eds), *Tectonics and Magmatism in Turkey and the Surrounding Area*. Geological Society, London, Special Publications 173, 2000, pp. 25–41.

[152] L. Beccaletto, C. Jenny, Geology and correlation of the Ezine zone: a Rhodope fragment in NW Turkey? *Turkish J. Earth Sci.* 13 (2004) 145–176.

[153] M. Duru, Ş. Pehlivan, Y. Şentürk, F. Yavaş, H. Kar, New results on the lithostratigraphy of the Kazdağ Massif in northwest Turkey, *Turkish J. Earth Sci.* 13 (2004) 177–186.

[154] A.İ. Okay, D. Altıner, Uppermost Triassic limestone in the Karakaya Complex– stratigraphic and tectonic significance, *Turkish J. Earth Sci.* 13 (2004) 187–199.

[155] A.İ. Okay, M.C. Göncüoğlu, The Karakaya Complex: a review of data and concepts, *Turkish J. Earth Sci.* 13 (2004) 75–95.

[156] E.A. Pickett, A.H.F. Robertson, Significance of the volcanogenic nilüfer unit and related components of the Triassic Karakaya Complex for Tethyan subduction/accretion processes in NW Turkey, *Turkish J. Earth Sci.* 13 (2004) 97–143.

[157] St.R. Taylor, S.M. McLennan, *The Continental Crust: its Composition and Evolution*, 1985, Blackwell Scientific Publications.